Liquid-solid impacts with compressible gas cushioning

PETER D. HICKS[1]†, AND RICHARD PURVIS[2]

[1]School of Engineering, Fraser Noble Building, King's College, University of Aberdeen, Aberdeen, AB24 3UE, UK

[2]School of Mathematics, University of East Anglia, Norwich, NR4 7TJ, UK

(Received ?; revised ?; accepted ?. - To be entered by editorial office)

Abstract: The role played by gas compressibility in gas cushioned liquid-solid impacts is investigated within a viscous gas and inviscid liquid regime. A full analysis of the energy conservation in the gas is conducted for the first time, which indicates that both thermal diffusion across the gas film and viscous dissipation play an important role in gas cushioning once gas compression becomes significant. Consequently existing models of gas compressibility based on either an isothermal or an adiabatic equation of state for the gas do not fully reflect the physics associated with this phenomena. Models incorporating thermal diffusion and viscous dissipation are presented, which are appropriate for length scales consistent with droplet impacts, and for larger scale liquid-solid impacts. The evolution of the free surface is calculated alongside the corresponding pressure, temperature and density profiles. These profiles indicate that a pocket of gas can become trapped during an impact. Differences between the new model and older models based on isothermal and adiabatic equations of state are discussed, along with predictions of the size of the trapped gas pocket.

Key words:

1. Introduction

Bubble trapping and capture is a commonly observed and important phenomena in many areas of violent impacts and water entry problems. Experiments have shown this in droplet impact with a rigid substrate (Thoroddsen *et al.* 2003; van Dam & Le Clerc 2004) as well as in solid impacts into water layers (Colagrossi *et al.* 2004; Abrahamsen & Faltinsen 2011). Applications are widespread from small length-scales of printing and spray coating, to larger length-scale engineering problems such as ship slamming and fluid sloshing. The underlying mechanism is common; the bubbles are formed by the narrowing gap between the water and solid producing a high pressure in the gas, which deforms the liquid free-surface, although depending on the typical length-scale either viscous or inertial forces in the air can be dominant. Rather than touchdown occurring at a single point (at the bottom of an approaching droplet, or at the minimum on an impinging solid), the air-cushioning forces the initial impact to occur instead at some positive horizontal distance away, and results in the capture of a gas pocket which goes on to form a bubble. Violent flows and impacts are much studied but the influence of the air is usually neglected entirely, although it is known to have significant influence on the pressure experienced by an impacting body (Chuang 1966; Takagi & Dobashi 2003), flow

† Email address for correspondence: p.hicks@abdn.ac.uk

dynamics in a sloshing tank (Rognebakke & Faltinsen 2005; Abrahamsen & Faltinsen 2011) and on the post-impact dynamics of droplet impacts (Xu *et al.* 2005). Investigations focusing on the role of gas-cushioning generally assume incompressible behaviour, although the parameter regimes and typical velocities involved for many applications suggest compressibility is important (Mandre *et al.* 2009; Hicks & Purvis 2012).

The earliest models of gas-cushioned liquid-solid impact, due to Smith *et al.* (2003), investigated liquid impact onto a solid in the presence of an incompressible isothermal gas layer. A scaling argument for the flow was developed for the cushioning phase, when the small vertical separation between the liquid and the substrate is much less than the horizontal extent of the interactions. This led to a model with a viscous lubrication equation for the gas layer behaviour and an inviscid description of the liquid. This model has been extended to three dimensions allowing predictions to be made for the size of the trapped bubble in terms of the approach speed U, and L the radius of curvature of either the undisturbed droplet or solid body at the point closest to impact (Hicks & Purvis 2010). These predictions are in good agreement with the available experimental data for droplet impacts. Recently the impact of a larger solid body with a locally spherical impact region and an initially stationary body of water has been investigated within the viscous gas and inviscid liquid regime. This again shows good agreement with the predicted air pocket radius, over a much wider range of parameters (Hicks *et al.* 2012).

Under the assumption that the gas behaves either isothermally or adiabatically when compressed Mandre *et al.* (2009) and Mani *et al.* (2010) extended the earlier models of droplet impact to incorporate gas compressibility, while providing an upper limit on the impact speed for which the gas may be considered incompressible. As with the incompressible case, when isothermal or adiabatic gas compression is included, the droplet free-surface deforms in response to the pressure build up in the viscous gas film, leading to the trapping of a gas bubble. The gas behaviour can be assumed to be adiabatic providing both the thermal diffusion and the viscous dissipation in the gas are small in comparison to both thermal advection and the work done by compression (Batchelor 1967). It is well known that these assumptions may not be valid in compressible viscous fluid flow, and in particular, Stewartson (1964) shows that viscous dissipation is significant within a compressible boundary layer flow; which like a thin film is a flow known for having a large discrepancy between the parallel and normal flow velocities. In the current investigation, it will be shown that thermal diffusion and viscous dissipation within the thin compressible viscous lubrication gas film are significant for liquid-solid impacts in many parameter regimes of interest including for droplet impacts.

High temperatures and pressures have been observed in many problems associated with bubble formation and bubble compression. The most extreme example of this is the phenomenon of sonoluminescence, where the compression of a bubble can produce temperatures of several thousand Kelvin for very short periods of time Brenner *et al.* (2002). Models of heat generation in sonoluminescence often neglect viscosity and assume the gas within the bubble behaves adiabatically. Within viscous fluids, the generation of heat through the viscous dissipation of energy has been previously studied in thin gas films in the context of a scroll compressor (Howell 2001). The distribution of energy has also been included when modelling post impact droplet behaviour (Bhardwaj *et al.* 2007; Bhardwaj & Attinger 2008).

The viscous gas and inviscid liquid regime is but one of many different types of cushioning in liquid-solid impacts. For higher momentum impacts the gas layer becomes inviscid like the droplet. This configuration has been investigated for an incompressible gas phase by Wilson (1991) and has applications in ship slamming and wave impacts. However, open questions remain regarding the stability of the models developed in this

case (see Oliver 2002; Purvis & Smith 2004). For lower momentum impacts viscous effects become important in the droplet as well as the gas, and rather than impact and splashing, the lower momentum regime describes droplet coalescence and spreading. In this regime Baldessari *et al.* (2007) and Kaur & Leal (2009) have investigated the free-surface evolution. Throughout the different momentum regimes, common features of the free-surface evolution are apparent, with the free surface evolving to capture a region of the separating fluid. If a second fluid phase separating the liquid free-surface and the impactor is not included and the liquid-solid impact is considered in a vacuum, as is typically the case in a classical Wagner theory (see e.g. Oliver 2002), then no pre-impact cushioning occurs and the liquid free-surface does not deform until after touchdown actually occurs.

In the current paper a full analysis of the energy conservation in an gas-cushioned liquid-solid impact is undertaken within the viscous gas and inviscid liquid regime, with the aim of assessing whether the gas really does behaves isothermally or adiabatically, or whether other effects such as thermal diffusion or viscous heating play a role in the evolution of energy. Prior to impact it is assumed that the liquid, gas and the solid are at the same ambient temperature. Note this assumption may not be valid in many physical situations, including ink-jet printing (where droplets are initially heated to aid their flow), and aircraft icing (where supercooled droplets strike heated aircraft surfaces (Gent *et al.* 2000)). However, this additional complication will not be considered here. In §2 a model is described that incorporates the conservation of energy in the gas, liquid and solid. These equations are non-dimensionalized and the leading-order behaviour is determined, by exploiting the small aspect ratio of the gas layer height to horizontal between the liquid and the solid immediately prior to impact. Although significant overlap exists between the parameter regimes, a model which is broadly appropriate to discussing air cushioning in droplet impacts is presented in §4, while a second model is presented in §5 that is appropriate for considering impacts of solid bodies into liquids at larger length scales. The model appropriate for droplet impacts is further divided into two sub-models: a model in which the gas is weakly compressible and a model in which the gas is fully compressible. Although only the fully compressible gas behaviour is considered in the case of solid body impacts into liquids, provisional results for weakly compressible case have previously been presented by Hicks & Purvis (2012). The similarities and differences between all these different models are discussed in §6, while also outlining methods through which these models could be further extended to cover wider parameter regimes.

2. Model equations and nondimensionalization

An idealized two dimensional problem is considered in which a solid body and a liquid are approaching impact, but remain separated by a dividing gas film. Attention will be restricted to droplet impacts and to solid body impacts into liquids. In the former case a frame of reference is considered in which the droplet moves towards a stationary substrate, while for solid body slamming, a frame of reference is considered in which the solid body moves towards an initially stationary liquid. A coordinate system $\boldsymbol{x} = (x, y)$ is used, with an origin on the substrate (undisturbed free-surface) directly below the centre of the droplet (solid body). The x direction lies parallel to either the substrate (in a droplet impact), or the undisturbed free-surface (in solid body slamming), while the y direction points upwards towards either the droplet or the solid body. Note, while it is straightforward to extend the model to describe gas cushioning in liquid-liquid collisions (see e.g. Hicks & Purvis 2011), in the current paper only gas cushioning in liquid-solid impacts is considered.

The velocity field is denoted $\boldsymbol{u} = (u, v)$. The liquid (with density ρ_l, temperature T_l and

pressure p_l), is separated from the wall by a region of gas (with density ρ_g, temperature T_g and pressure p_g). Here and subsequently, a subscript l is used to denote a property of the liquid and a subscript g is used to denote a property of the gas. The solid body has the thermal properties of glass, to match many of the experiments, although our findings are insensitive to the exact thermal properties of the solid and hold for most common materials. In particular the solid has a density ρ_s and a temperature T_s, where the subscript s denotes a property of the solid phase.

In the gas film, conservation of mass, momentum and energy can be written as

$$\frac{\partial \rho_g}{\partial t} + \nabla \cdot (\rho_g \boldsymbol{u}_g) = 0, \tag{2.1a}$$

$$\rho_g \left(\frac{\partial \boldsymbol{u}_g}{\partial t} + \boldsymbol{u}_g \cdot \nabla \boldsymbol{u}_g \right) = -\nabla p_g + \nabla \cdot (\mu_g \nabla \boldsymbol{u}_g) + \nabla \left[(\mu_g + \lambda_g) \nabla \cdot \boldsymbol{u}_g \right], \tag{2.1b}$$

$$\rho_g c_{v,g} \left(\frac{\partial T_g}{\partial t} + \boldsymbol{u}_g \cdot \nabla T_g \right) = -p_g \nabla \cdot \boldsymbol{u}_g + k_g \nabla^2 T_g + \Phi_g, \tag{2.1c}$$

where μ_g and λ_g are the shear and dilatational viscosities, respectively; k_g is the thermal conductivity and $c_{v,g}$ is the specific heat capacity at constant volume of the gas. In practical situations, both the thermal conductivity and the specific heat capacity will have a weak dependence upon temperature. However, if the model of Rohsenow *et al.* (1998, section 2.4) for the dependence of thermal conductivity upon temperature in dry air is used, then (for the case describe by figure 2), the maximum variation in thermal conductivity is less than 9% and this only occurs for a very small portion of the impact. Consequently both the thermal conductivity and the specific heat capacity are assumed to be constant throughout. The terms in the energy conservation equations, correspond to the rate of change of thermal energy, work done by pressure, diffusion of heat and viscous dissipation. In the conservation laws for the gas, it is assumed that the thermal properties of the gas are constant, while the viscosities are allowed to vary with temperature. The viscous dissipation term is given by

$$\Phi_g = \mu_g \left[2 \left(\frac{\partial u_g}{\partial x} \right)^2 + 2 \left(\frac{\partial v_g}{\partial y} \right)^2 + \left(\frac{\partial u_g}{\partial y} + \frac{\partial v_g}{\partial x} \right)^2 \right] + \lambda_g \left(\nabla \cdot \boldsymbol{u}_g \right)^2. \tag{2.1d}$$

In a viscous gas film, it is expected that the kinetic energy imparted to the gas film will be dissipated as heat, raising its temperature. To close the model an equation of state is required. If the gas behaves like a perfect gas, then the equation of state is given by the ideal gas law

$$p_g = \rho_g R_g T_g, \tag{2.1e}$$

where the specific gas constant $R_g = c_{p,g} - c_{v,g}$, while $c_{p,g}$ is the specific heat capacity at constant pressure.

The gas shear viscosity is independent of pressure, but it does depends on temperature through Sutherland's formula (see e.g. Stewartson 1964)

$$\mu_g = \mu_0 \frac{T_{g,0} + C}{T_g + C} \left(\frac{T_g}{T_{g,0}} \right)^{3/2}, \tag{2.2}$$

where $\mu_0 = 1.827 \times 10^{-5}\,\mathrm{Pa\,s}$, a reference viscosity (in this case for air), measured at a reference temperature $T_{g,0} = 291.15\,\mathrm{K}$. The parameter C is Sutherland's constant for the material in the gas film, and takes the value 120 K if that gas is air. In principle, the dependence of the dilatational viscosity on temperature should also be specified. This dependence is harder to quantify. However, in a thin gas film of small aspect ratio, it

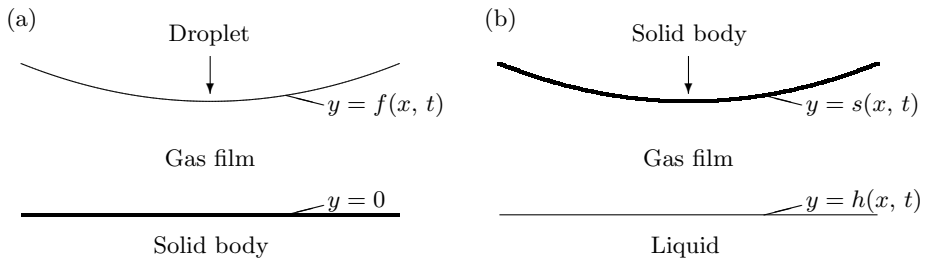

FIGURE 1. Two situations where a gas bubble may become trapped during a liquid-solid impact: (a) a droplet approaching impact with a rigid body and (b) a solid body approaching impact with a liquid. In both diagrams a thick solid line indicates a rigid surface, while a thin solid line indicates a liquid-gas interface, which can evolve over time.

will subsequently be shown that the leading order behaviour does not depend on the dilatational viscosity at all, providing the shear and dilatational viscosities are of the same order of magnitude. Therefore there is no need to specify how the dilatational viscosity depends on temperature.

If the liquid is incompressible, then conservation of mass, momentum and energy can be written as

$$\nabla \cdot \boldsymbol{u}_l = 0, \tag{2.3a}$$

$$\rho_l \left(\frac{\partial \boldsymbol{u}_l}{\partial t} + \mathbf{u}_l \cdot \nabla \boldsymbol{u}_l \right) = -\nabla p_l + \nabla \cdot (\mu_l \nabla \boldsymbol{u}_l), \tag{2.3b}$$

$$\rho_l c_{p,l} \left(\frac{\partial T_l}{\partial t} + \boldsymbol{u}_l \cdot \nabla T_l \right) = k_l \nabla^2 T_l + \Phi_l, \tag{2.3c}$$

where μ_l is the shear viscosity, $c_{p,l}$ the specific heat at constant pressure and k_l the thermal conductivity of the liquid. In principle, the shear viscosity of the liquid may again depend upon temperature. However, again it shall be shown that to leading order the behaviour of the gas is inviscid, allowing this complication to be neglected. As the liquid is incompressible the viscous dissipation of energy takes the simpler form

$$\Phi_l = \mu_g \left[2 \left(\frac{\partial u_l}{\partial x} \right)^2 + 2 \left(\frac{\partial v_l}{\partial y} \right)^2 + \left(\frac{\partial u_l}{\partial y} + \frac{\partial v_l}{\partial x} \right)^2 \right]. \tag{2.3d}$$

The solid body involved in the liquid-solid body is assumed to be rigid. However, if the temperature can change in both the gas film and the liquid droplet, then it may also be able to change in the solid. Energy conservation in the solid implies

$$\rho_s c_{p,s} \frac{\partial T_s}{\partial t} = k_s \nabla^2 T_s, \tag{2.4}$$

where $c_{p,s}$ is the specific heat capacity at constant pressure and k_s is the thermal conductivity of the solid.

Next the appropriate boundary conditions on both the free surface and the boundary of the solid body must be considered. It is assumed that a single, stable interface between the liquid and gas phases exists throughout the pre-impact gas cushioning and that detached small droplets and bubbly regions containing a mixture of liquid and gas are not formed. This is consistent with the experimental observations of droplet impacts (Thoroddsen *et al.* 2003) and also of moderate length-scale slamming body impacts

into liquid (Hicks *et al.* 2012), which motivate this study. However, this contrasts with behaviour observed for much larger bodies and higher impact speeds (as seen in ship slamming), where the additional gas inertia produces free-surface instabilities that can lead to small droplet ejecta and regions of entrained bubbles close to the liquid-gas boundary. Initially the position of upper boundary of the gas film is written as $y = f_+(x, t)$, while the position of the lower boundary is written as $y = f_-(x, t)$. Here (and subsequently), the subscript $+$ indicates a property of the upper boundary of the gas layer, while the subscript $-$ indicates a property of the lower boundary of the gas layer. During an impact of a droplet approaching a solid body (as shown in figure 1(a)), the upper $+$ interface takes the properties of the liquid droplet, while the lower $-$ interface takes the properties of the solid body. Conversely as a solid body approaches impact with an initially stationary liquid (as shown in figure 1(b)), the upper $+$ interface takes the properties of the solid, while the lower $-$ interface takes the properties of the liquid. In a droplet impact, the upper boundary is free to deform and is denoted $y = f_+(x, t) = f(x, t)$, while the lower boundary is rigid and is given by $y = f_-(x, t) = 0$. For the impact of a solid body into liquid the solid is rigid, although it does move towards the liquid with the position of its boundary being denoted $y = f_+(x, t) = s(x, t)$, while the liquid interface at the below the gas film is able to deform and has position $y = f_-(x, t) = h(x, t)$.

No-slip and no-penetration boundary conditions are required on the boundary of the solid body. On the free surface the kinematic boundary conditions are applied in both the liquid and gas phases, while the pressure is coupled across the free surface through the balance of normal stresses. It is assumed that no evaporation or other phase change phenomena occurs over the very short time scale associated with the liquid-solid impact, so that energy conservation at both the gas-liquid and gas-solid boundaries implies

$$k_g \nabla T_g \cdot \boldsymbol{n}_\pm = k_\pm \nabla T_\pm \cdot \boldsymbol{n}_\pm, \tag{2.5}$$

conserving the heat flux across each interface.

The problem of a droplet or solid body with undisturbed radius of curvature L, approaching impact from the normal direction with velocity U will be considered. When combined with the liquid density ρ_l and a liquid viscosity μ_l, this gives a Reynolds number for the liquid, $Re = \rho_l U L/\mu_l$. For a water droplet with radius $L = 1\,\mathrm{mm}$ and an approach speed $U = 1\,\mathrm{m\,s^{-1}}$, the Reynolds number $Re = 1000$, while for a solid body of radius $L = 0.5\,\mathrm{m}$ and an approach speed $U = 0.1\,\mathrm{m\,s^{-1}}$, the corresponding Reynolds number $Re = 49,900$ when calculated using the properties of water. Next equations are developed for the gas film where it shall be shown that the gas viscosity cannot be neglected in the regime of interest.

2.1. *Gas film*

As impact approaches the viscous forces in the gas are initially too small to influence the bulk liquid flow, until the gas layer becomes thin enough to induce gas pressures which are comparable to the inertial flow in the liquid phase. Consequently, a non-dimensional scaling will be chosen which focus on this thin region. A horizontal length scale εL is used, which is based on the droplet or solid body radius L and a small parameter ε, the value of which has yet to be determined. Very close to impact the separation between the droplet and impactor is smaller than even this horizontal length scale, so a vertical length scale $\varepsilon^2 L$ is used. A corresponding time scale is chosen, which would allow the motion of the droplet or the solid body to close the gap if the motion of the droplet or

the body is not retarded and the liquid free-surface does not deform. Written together this scaling implies

$$(x,\, y,\, f_{\pm},\, t) = \left(\varepsilon L x',\, \varepsilon^2 L y',\, \varepsilon^2 L f'_{\pm},\, \frac{\varepsilon^2 L}{U} t'\right), \tag{2.6a}$$

where the primes are used to denote dimensionless quantities. In order to preserve mass conservation, the additional factor of ε in the vertical length scale results in a similar difference between the horizontal and vertical velocities. The increase in the gas pressure over the ambient gas pressure p_0 is $\varepsilon^{-1}\rho_l U^2$, where the liquid density ρ_l is used to match the pressure in the droplet and the ε factor retains the gas pressure at leading order. Taken together, alongside a non-dimensionalization for the gas density and temperature,

$$(u_g,\, v_g,\, p_g,\, \rho_g,\, T_g) = \left(\frac{U}{\varepsilon} u'_g,\, U v'_g,\, p_0 + \frac{\rho_l U^2}{\varepsilon} p'_g,\, [\rho_g]\, \rho'_g,\, T_0 + [T]\, T'_g\right). \tag{2.6b}$$

Here, the gas density scale $[\rho_g]$ and the change in gas temperature $[T]$, are both determined by the ideal gas law (2.1*e*), and have the form

$$[\rho_g] = \frac{p_0}{R_g T_0}, \quad \text{and} \quad [T] = \frac{\rho_l U^2}{\varepsilon} \frac{1}{R_g\, [\rho_g]}, \tag{2.6c}$$

where the ambient temperature is denoted T_0. Finally, to complete the gas film non-dimensionalization, scalings are required for the viscosities and the viscous dissipation term in the energy conservation equation. These are taken to be

$$(\mu_g,\, \lambda_g,\, \Phi_g) = \left(\mu_0 + [\mu_g]\, \mu'_g,\, \lambda_0 + [\mu_g]\, \lambda'_g,\, [\Phi_g]\, \Phi'_g\right). \tag{2.6d}$$

If this non-dimensionalization is substituted into the equations governing the gas (and the primes signifying non-dimensional variables are dropped for convenience), then the mass conservation equation for the gas (2.1*a*) implies

$$\frac{\partial \rho_g}{\partial t} + \frac{\partial}{\partial x}\left(\rho_g u_g\right) + \frac{\partial}{\partial y}\left(\rho_g v_g\right) = 0. \tag{2.7}$$

If the small parameter ε is chosen to be

$$\varepsilon = \left(\frac{\mu_0}{\mu_l Re}\right)^{1/3} = \left(\frac{\mu_0}{\mu_l} \frac{\mu_l}{\rho_l U L}\right)^{1/3}, \tag{2.8}$$

then the pressure gradient in the horizontal momentum conservation equation balances the largest viscous term.

In the equation governing viscous dissipation (2.1*d*), the leading order behaviour is given by

$$[\Phi_g]\, \Phi_g \sim \frac{\mu_0 U^2}{\varepsilon^6 L^2} \left(1 + m\mu_g\right) \left(\frac{\partial u_g}{\partial y}\right)^2 + O\left(\varepsilon^{-4}\right), \tag{2.9}$$

where $m = [\mu_g]\, / \mu_0$. Subsequently the viscous dissipation scaling is taken to be

$$[\Phi_g] = \frac{\mu_0 U^2}{\varepsilon^6 L^2}, \tag{2.10}$$

and in conjunction with the temperature scale (2.6*c*), this implies the energy conservation

equation (2.1*c*) can be written as

$$\rho_g \left(\frac{\partial T_g}{\partial t} + \boldsymbol{u}_g \cdot \nabla T_g \right) - \frac{\gamma - 1}{\gamma} \left(\frac{\partial p_g}{\partial t} + \boldsymbol{u}_g \cdot \nabla p_g \right) = \frac{1}{\varepsilon^2 Pe_g} \left(\varepsilon^2 \frac{\partial^2 T_g}{\partial x^2} + \frac{\partial^2 T_g}{\partial y^2} \right) + \frac{\gamma - 1}{\gamma} (1 + m\mu_g) \left(\frac{\partial u_g}{\partial y} \right)^2 . \quad (2.11)$$

where the gas Péclet number is defined to be

$$Pe_g = \frac{[\rho_g]\, c_{p,g} U L}{k_g}, \quad (2.12)$$

and

$$K = \frac{\rho_l U^2}{p_0}. \quad (2.13)$$

Here $\varepsilon^{-1}K$ is the ratio of the gas pressure increase in the gas induced by the approaching impact to the ambient gas pressure and measures the importance of gas compressibility. If $\varepsilon^{-1}K \ll 1$, then the pressure induced in the viscous gas is much smaller the ambient gas pressure and to a good level of approximation the gas can be considered to be incompressible. Alternatively the pressure induced in the gas is either approximately equal to, or is much greater than, the ambient gas pressure and effects due to the compressibility of the gas are significant.

If the terms on the right-hand side of (2.11), corresponding to thermal diffusion and viscous dissipation are negligible, then the gas flow would be adiabatic and the energy conservation equation simplifies to

$$\frac{D}{Dt} \left(\frac{1 + \varepsilon^{-1} K p_g}{\rho_g^{\gamma}} \right) = 0, \quad (2.14)$$

so that

$$\rho_g = \left(1 + \varepsilon^{-1} K p_g \right)^{1/\gamma}. \quad (2.15)$$

This simplified equation of state, which does not include an explicit temperature dependence, was used by Mandre *et al.* (2009) and Mani *et al.* (2010) to model compressible gas behaviour in droplet impacts with adiabatic ($\gamma = 1.4$) and isothermal ($\gamma = 1$) gas compression. However, the terms on the right-hand side of (2.11) may not be small. In particular, for a droplet with radius $L = 1\,\mathrm{mm}$ and an approach speed $U = 1\,\mathrm{m\,s^{-1}}$, the reduced Péclet number in the gas, $\varepsilon^2 Pe_g = 0.01$, while $Pe_g = 47$. Similarly for an impact of a solid body with radius of curvature $L = 0.5\,\mathrm{m}$ and an approach speed towards an initially stationary body of water $U = 0.1\,\mathrm{m\,s^{-1}}$, $\varepsilon^{-2} Pe_g = 0.11$, while $Pe_g = 2347$. Therefore in the parameter range of interest the right hand side of (2.11) is not small and should not be neglected. In fact, to leading order, the thermal diffusion across the gas film dominates the energy conservation equation.

If either the thermal diffusion and viscous dissipation terms are retained, then the temperature must be explicitly retained, and the full equation of state (2.1*e*) non-dimensionalizes to give

$$1 + \varepsilon^{-1} K p_g = \rho_g \left(1 + \varepsilon^{-1} K T_g \right). \quad (2.16)$$

Hence, the leading order behaviour is governed by the size of $\varepsilon^{-1}K$. If $\varepsilon^{-1}K \ll 1$, then in addition to the gas being incompressible, it is also isothermal. Conversely, if $\varepsilon^{-1}K \sim 1$, or $\varepsilon^{-1}K \gg 1$, then thermal effects are important in the gas, as well as the gas being

compressible. In non-dimensional variables, the viscosity depends on the gas temperature through

$$1 + m\mu_g = \frac{\Theta\left(1 + \varepsilon^{-1}KT_g\right)^{3/2}}{\left(1 + \Pi + \varepsilon^{-1}KT_g\right)}, \tag{2.17}$$

where $\Pi = [\rho_g]\, R_g C/p_0$, and $\Theta = T_0^{1/2}\left(T_{g,0} + C\right)/T_{g,0}^{3/2}$. At an ambient pressure $p_0 = 100000\,\mathrm{Pa}$ and temperature $T_0 = 300\,\mathrm{K}$, $\Pi = 0.4$ and $\Theta = 1.433$. Therefore in the limit $\varepsilon^{-1}K \ll 1$ the gas viscosity is independent of temperature to leading order.

2.2. *Liquid and solid wall*

The behaviour of the liquid over the very short time scales envisaged for gas cushioning is of interest. Close to the point of impact the horizontal and vertical length scales associated with the liquid remain roughly comparable, unlike in the gas film. The gas flow drives a flow in the liquid phase and is expected to initially induce variations in the free-surface position of order ε. Therefore

$$(x,\, y,\, f_\pm,\, t) = \left(\varepsilon L x',\, \varepsilon L y',\, \varepsilon^2 L f'_\pm,\, \frac{\varepsilon^2 L}{U} t'\right). \tag{2.18a}$$

To satisfy conservation of liquid mass the scaling on the horizontal and vertical velocity components must be equal and this is taken to be the approach velocity U. The pressure and temperature in the liquid is chosen to match that in the gas film in order to couple the behaviour of the droplet and the gas film. Together with a non-dimensionalization for the viscous dissipation term

$$(u_l,\, v_l,\, p_l,\, T_l,\, \Phi_l) = \left(U u'_l,\, U v'_l,\, p_0 + \frac{\rho_l U^2}{\varepsilon} p'_l,\, T_0 + [T]\, T'_l,\, \frac{\mu_l U^2}{\varepsilon^2 L^2}\Phi'_l\right). \tag{2.18b}$$

Applying this non-dimensionalization to the governing equations for the liquid (2.3), and immediately dropping the dashes results in

$$\nabla \cdot \boldsymbol{u}_l = 0, \tag{2.19a}$$

$$\frac{\partial \boldsymbol{u}_l}{\partial t} + \varepsilon \boldsymbol{u}_l \cdot \nabla \boldsymbol{u}_l = -\nabla p_l + \frac{1}{Re}\nabla^2 \boldsymbol{u}_l, \tag{2.19b}$$

$$\frac{\partial T_l}{\partial t} + \varepsilon \boldsymbol{u}_l \cdot \nabla T_l = \frac{1}{Pe_l}\nabla^2 T_l + \frac{Br_l}{Pe_l}\Phi_l, \tag{2.19c}$$

where the non-dimensional Péclet and Brinkman numbers in the liquid are defined to be

$$Pe_l = \frac{\rho_l c_{p,l} U L}{k_l}, \quad \text{and} \quad Br_l = \frac{\mu_l U^2}{k_l\,[T]} = \frac{\varepsilon \mu_l R_g\,[\rho_g]}{k_l \rho_l}, \tag{2.20}$$

respectively. For a droplet with radius $L = 1\,\mathrm{mm}$ and an approach speed $U = 1\,\mathrm{m\,s^{-1}}$, $Pe_l = 7000$ and $Br_l = 1.5{\times}10^{-5}$; while for a solid body with $L = 0.5\,\mathrm{m}$ and $U = 0.1\,\mathrm{m\,s^{-1}}$, $Pe_l = 8.7 \times 10^4$ and $Br_l = 1.7 \times 10^{-9}$, indicating viscous heating can be neglected in the liquid.

The solid body is assumed to be rigid and isotropic with respect the thermal conductivity. However, as the heat flux from the gas film may transfer energy into the solid, the conservation of energy must be considered within the solid. The vertical extent of the solid is assumed to be at least εL and therefore length scales within the solid are given by equation (2.18*a*). It should be noted that if the vertical extent of the solid material is small compared to εL (which would correspond to a thin solid layer), then a more complicated analysis of the energy conservation in the solid is required. In the solid the

temperature is scaled with

$$T_s = T_0 + [T]\, T_s', \tag{2.21}$$

to match the gas temperature. When applied to the energy conservation equation in the solid (2.4),

$$\frac{\partial T_s}{\partial t} = \frac{1}{Pe_s}\nabla^2 T_s, \tag{2.22}$$

where the Péclet number for the solid is

$$Pe_s = \frac{\rho_s c_{p,s} U L}{k_s}. \tag{2.23}$$

Assuming the solid has the properties of glass, then for a droplet with radius $L = 1\,\mathrm{mm}$ and an approach speed $U = 1\,\mathrm{m\,s^{-1}}$ the corresponding Péclet number, $Pe_s = 1770$; while for a solid body with $L = 0.5\,\mathrm{m}$ and $U = 0.1\,\mathrm{m\,s^{-1}}$, $Pe_s = 1 \times 10^5$.

2.3. *Interface conditions*

The non-dimensionalization of the no-slip, no-penetration and kinematic boundary conditions remain unchanged from their counterparts in the incompressible case. The normal stress balance across the free-surface is modified due to gas compressibility. However, the additional terms corresponding to gas compressibility are not present at leading order in ε and for brevity the full non-dimensional normal stress balance is not included at this stage.

The non-dimensional gas-liquid and gas-solid thermal conductivity ratios are defined to be

$$\lambda_{gl} = \frac{k_g}{k_l}, \quad \text{and} \quad \lambda_{gs} = \frac{k_g}{k_s}, \tag{2.24}$$

respectively. For air, water and glass the values of $\lambda_{gl} = 0.042$ and $\lambda_{gs} = 0.022$. Now energy conservation across the interfaces (2.5) implies

$$\frac{\lambda_{g\pm}}{\varepsilon}\left(\frac{\partial T_g}{\partial y} - \varepsilon^2 \frac{\partial f_\pm}{\partial x}\frac{\partial T_g}{\partial x}\right) = \frac{\partial T_\pm}{\partial y} - \varepsilon \frac{\partial f_\pm}{\partial x}\frac{\partial T_\pm}{\partial x}. \tag{2.25}$$

3. Small ε asymptotic behaviour

The momentum and energy conservation equations in the gas involve the small parameter ε. To exploit this small parameter, asymptotic expansions of the gas velocity components, pressure, density, viscosity and film height are proposed with the form

$$\begin{aligned}(u_g,\, v_g,\, p_g,\, \rho_g,\, \mu_g,\, f_\pm) = &\left(u_g^{(0)},\, v_g^{(0)},\, p_g^{(0)},\, \rho_g^{(0)},\, \mu_g^{(0)},\, f_\pm^{(0)}\right) \\ &+ \varepsilon\left(u_g^{(1)},\, v_g^{(1)},\, p_g^{(1)},\, \rho_g^{(1)},\, \mu_g^{(1)},\, f_\pm^{(1)}\right) + O\left(\varepsilon^2\right).\end{aligned} \tag{3.1}$$

To leading order in ε, the gas mass conservation equation (2.7) implies

$$\frac{\partial \rho_g^{(0)}}{\partial t} + \frac{\partial}{\partial x}\left(\rho_g^{(0)} u_g^{(0)}\right) + \frac{\partial}{\partial y}\left(\rho_g^{(0)} v_g^{(0)}\right) = 0. \tag{3.2}$$

Similarly, in gas momentum conservation equations (2.1*b*), if

$$\frac{[\rho_g]}{\rho_l} \ll \varepsilon, \tag{3.3}$$

then gas inertia can be neglected and to leading order

$$0 = -\frac{\partial p_g^{(0)}}{\partial x} + \frac{\partial}{\partial y}\left[\left(1 + m\mu_g^{(0)}\right)\frac{\partial u_g^{(0)}}{\partial y}\right], \tag{3.4a}$$

$$0 = -\frac{\partial p_g^{(0)}}{\partial y}. \tag{3.4b}$$

The vertical momentum conservation equation (3.4*b*) immediately implies that the gas pressure does not vary across the gas film, so that $p_g^{(0)} = p_g^{(0)}(x, t)$. Subsequently to leading order, (3.4) implies the gas flow is governed by a lubrication equation.

Similarly in the liquid the velocity components and the pressure are again expanded in terms of the small parameter ε by taking asymptotic expansion with the form

$$(u_l, v_l, p_l) = \left(u_l^{(0)}, v_l^{(0)}, p_l^{(0)}\right) + \varepsilon\left(u_l^{(1)}, v_l^{(1)}, p_l^{(1)}\right) + O\left(\varepsilon^2\right). \tag{3.5}$$

As $Re \gg 1$, to leading order, the liquid droplet is inviscid and its behaviour is governed by the linearized Euler equations

$$\nabla \cdot \boldsymbol{u}_l^{(0)} = 0, \quad \text{and} \quad \frac{\partial \boldsymbol{u}_l^{(0)}}{\partial t} = -\nabla p_l^{(0)}. \tag{3.6}$$

This implies that the liquid pressure (and in particular derivatives of pressure with respect to x), are solutions of the Laplace equation.

In the kinematic boundary conditions on the liquid interface imply

$$v_l^{(0)} = \frac{\partial f_+^{(0)}}{\partial t}, \quad \text{as} \quad y \searrow 0, \tag{3.7a}$$

and

$$v_l^{(0)} = \frac{\partial f_-^{(0)}}{\partial t}, \quad \text{as} \quad y \nearrow 0, \tag{3.7b}$$

to leading order. Similarly the normal stress balance implies

$$p_{\pm l}^{(0)} - p_g^{(0)} = \mp\frac{\varepsilon}{We}\frac{\partial^2 f_\pm^{(0)}}{\partial x^2} + O\left(\varepsilon^2\right), \quad \text{on} \quad y = f_\pm^{(0)}. \tag{3.8}$$

Here the Weber number $We = \rho_l U^2 L/\sigma$, where σ denotes the surface tension. For a droplet with radius $L = 1\,\mathrm{mm}$ and approach speed $U = 1\,\mathrm{m\,s^{-1}}$, the Weber number $We = 14$, while for a solid body with radius $L = 0.5\,\mathrm{m}$ and approach speed $U = 0.1\,\mathrm{m\,s^{-1}}$, the Weber number $We = 69$. Consequently as $\varepsilon \ll 1$, surface tension effects can be neglected within the problem, except perhaps at the final instants prior to touchdown when a cusp appears to form on the free surface, and locally $f_{\pm,xx}^{(0)} = O\left(\varepsilon^{-1}\,We\right)$. Consequently the pressure in the gas as it approaches the interface equals the pressure in the liquid at that point. Subsequently this common leading-order pressure is denoted $p^{(0)}$, coupling the behaviour of the gas film to the behaviour of the liquid.

Using either complex variable methods (Smith *et al.* 2003) or Green's functions (Wilson 1991), the acceleration of the free surface can now be written as a principle valued integral of the pressure over the free surface, with the form

$$\frac{\partial^2 f_\pm^{(0)}}{\partial t^2} = \pm\frac{1}{\pi}\fint_{-\infty}^{\infty}\frac{\partial p^{(0)}}{\partial \xi}\frac{d\xi}{\xi - x}. \tag{3.9}$$

Here the kinematic boundary condition (3.7) has been used to introduce $f_{\pm}^{(0)}$.

The temperatures in the gas, liquid and solid are expanded in the form

$$(T_g,\, T_l,\, T_s) = \left(T_g^{(0)},\, T_l^{(0)},\, T_s^{(0)}\right) + \varepsilon\left(T_g^{(1)},\, T_l^{(1)},\, T_s^{(1)}\right) + O\left(\varepsilon^2\right), \tag{3.10}$$

in order to keep the temperature variations the same size in each of the gas, liquid and solid phases. Across the boundary of the gas film the heat flux boundary condition is given by (2.25). If $\Lambda_{g\pm} = \varepsilon^{-1}\lambda_{g\pm} = O(1)$, then matching coefficients at $O(1)$, $O(\varepsilon)$ and $O\left(\varepsilon^2\right)$ gives

$$\Lambda_{g\pm}\frac{\partial T_g^{(0)}}{\partial y} = \frac{\partial T_{\pm}^{(0)}}{\partial y}, \tag{3.11a}$$

$$\Lambda_{g\pm}\frac{\partial T_g^{(1)}}{\partial y} = \frac{\partial T_{\pm}^{(1)}}{\partial y} - \frac{\partial f_{\pm}^{(0)}}{\partial x}\frac{\partial T_{\pm}^{(0)}}{\partial x}, \tag{3.11b}$$

and

$$\Lambda_{g\pm}\left(\frac{\partial T_g^{(2)}}{\partial y} - \frac{\partial f^{(0)}}{\partial x}\frac{\partial T_g^{(0)}}{\partial x}\right) = \frac{\partial T_{\pm}^{(2)}}{\partial y} - \frac{\partial f_{\pm}^{(0)}}{\partial x}\frac{\partial T_{\pm}^{(1)}}{\partial x} - \frac{\partial f_{\pm}^{(1)}}{\partial x}\frac{\partial T_{\pm}^{(0)}}{\partial x}, \tag{3.11c}$$

respectively. If a droplet of radius $L = 1\,\mathrm{mm}$ and approach speed $U = 1\,\mathrm{m\,s^{-1}}$, impacting a solid with the thermal properties of glass, then $\Lambda_{gl} = 1.59$ and $\Lambda_{gl} = 0.86$. Similarly for a solid body with radius $L = 0.5\,\mathrm{m}$ and approach speed $U = 0.1\,\mathrm{m\,s^{-1}}$, $\Lambda_{gl} = 5.92$ and $\Lambda_{gs} = 3.55$ and therefore $\Lambda_{g\pm} = O(1)$ in the parameter regime of interest.

In the liquid energy conservation equation (2.19c), if $Pe_l^{-1} = O\left(\varepsilon^2\right)$ and $Br_l Pe_l^{-1} \ll \varepsilon^2$, then matching coefficients at $O\left(\varepsilon^0\right)$ implies

$$T_l^{(0)}(x,\, y,\, t) = 0. \tag{3.12}$$

Proceeding inductively to higher powers of ε implies

$$T_l^{(1)}(x,\, y,\, t) = T_l^{(2)}(x,\, y,\, t) = 0, \tag{3.13}$$

indicating that there is no temperature increase in the liquid droplet over the very short time scales associated with cushioning. Similarly in the solid,

$$T_s^{(0)}(x,\, y,\, t) = T_s^{(1)}(x,\, y,\, t) = T_s^{(2)}(x,\, y,\, t) = 0, \tag{3.14}$$

as $Pe_s^{-1} = O(\varepsilon)$. The liquid and solid retain the ambient temperature over the gas cushioning time-scale because this is much shorter than the time scale associated with thermal diffusion into either the liquid or solid.

Together the boundary conditions (3.11), and temperature fields (3.12), (3.13) and (3.14) imply

$$\frac{\partial T_g^{(0)}}{\partial y} = 0, \quad \text{on} \quad y = f_{\pm}^{(0)}, \tag{3.15a}$$

$$\frac{\partial T_g^{(1)}}{\partial y} = 0, \quad \text{on} \quad y = f_{\pm}^{(0)}, \tag{3.15b}$$

$$\frac{\partial T_g^{(2)}}{\partial y} = \frac{\partial f_{\pm}^{(0)}}{\partial x}\frac{\partial T_g^{(0)}}{\partial x}, \quad \text{on} \quad y = f_{\pm}^{(0)}. \tag{3.15c}$$

Hence as both the solid and the liquid phase temperatures are constant, the gas film is insulated and any heat created in the gas film is unable to escape.

TABLE 1. Values of non-dimensional parameters at an ambient pressure $p_0 = 100000$ Pa and temperature $T_0 = 300$ K, corresponding to weakly compressible gas flow (with $K \sim \varepsilon^2$), and compressible gas flow ($K \sim \varepsilon$) for droplet impacts (with $Pe_g = O(1)$) and solid body impacts into liquids (with $\varepsilon Pe_g = O(1)$). The numbers highlighted in bold indicate the $O(1)$ parameters in each of the distinguished limits.

	Droplet impacts		Solid-body impacts		
	Weakly compressible	Compressible	Weakly compressible	Compressible	
L	0.0005	0.0002	0.4	0.05	m
U	0.3	1	0.05	0.5	$\mathrm{m\,s^{-1}}$
ε	0.049	0.044	0.010	0.009	
K	0.0009	0.01	2.5×10^{-5}	0.0025	
$\varepsilon^{-1}K$	0.018	**0.23**	0.003	**0.28**	
$\varepsilon^{-2}K$	**0.378**	5.09	**0.274**	31.8	
Pe_g	**7.04**	**9.39**	938.8	1173.5	
εPe_g	0.343	0.416	**8.962**	**10.4**	
Re	150	200	19960	24950	
We	0.625	2.78	13.88	173.61	
Pe_l	1045	1393	1.4×10^5	1.7×10^5	
Pe_s	532	1773	4.2×10^4	5.3×10^4	
Br_l	2×10^{-11}	2×10^{-10}	6×10^{-13}	6×10^{-11}	
Λ_{gs}	0.51	0.56	2.61	2.82	
Λ_{gl}	0.85	0.94	4.36	4.70	

If the equation of state for the gas (2.16) is used to eliminate the gas density ρ_g from the gas energy conservation (2.11), then the resulting equation contains five different non-dimensional parameters: γ, m, ε, K and Pe_g. Of these parameters the ratio of specific heats $\gamma = 1.4$ for air, while the ratio of viscosities m is also an $O(1)$ property for air and these quantities are not affected by the impact speed and length scale. The remaining three non-dimensional parameters only ever explicitly appear in one of two larger non-dimensional groups: a reduced Péclet number $\varepsilon^2 Pe_g$ and a compressibility parameter $\varepsilon^{-1}K$, both of which depend upon the impact approach speed U and the length scale L. To determine the leading-order behaviour of the gas energy equation, it is necessary to consider the relative size of the groups $\varepsilon^2 Pe_g$ and $\varepsilon^{-1}K$ compared to powers of ε. For smaller droplet impacts $Pe_g = O(1)$, while for solid body impacts into water $\varepsilon Pe_g = O(1)$. Similarly two different regimes will be considered for the gas compressibility parameter: $\varepsilon^{-1}K = O(1)$ for which the gas is compressible and $\varepsilon^{-1}K \ll 1$ for which the gas is incompressible. In the incompressible case the particular limit $\varepsilon^{-2}K = O(1)$ is considered for which the gas is weakly compressible. Given two pairs of different parameter regimes, four different distinguished limits are identified corresponding to: compressible gas-cushioned droplet impacts, weakly-compressible gas-cushioned droplet impacts, compressible gas-cushioned solid body impacts into liquids and weakly compressible gas-cushioned solid body impacts into liquids. The first three of these limits are discussed in the following section while the case corresponding to weakly compressible solid body impacts into liquids was previously considered by Hicks & Purvis (2012). Typical values of the approach speed U and length scale L that give rise to each distinguished limit are shown in table 1.

Subsequently all impacts for which $Pe_g = O(1)$ are all described as droplet impacts, while all impacts for which $\varepsilon Pe_g = O(1)$ are described as solid body impacts into liquid. However, this distinction is made solely for clarity of presentation and given the impact of a solid body whose dimensions roughly match those of a droplet (such as in the experiments by Marston *et al.* (2011)), then the cushioning may be more accurately described by the $Pe_g = O(1)$ model, while for very large droplets with radii of 2 mm and impact speeds in excess of $1\,\mathrm{m\,s^{-1}}$ the $\varepsilon Pe_g = O(1)$ model can be more appropriate.

The four distinguished limits described do not cover the full range of applications in which one can find gas-cushioned liquid-solid impacts. Mandre *et al.* (2009) and Mani *et al.* (2010) investigate a highly compressible gas-cushioned droplet impact regime (albeit with a adiabatic equation of state), which corresponds to $\varepsilon^{-1}K \gg 1$ in the current notation. Additionally for very large bodies at high speed $\varepsilon^2 Pe_g$ can be $O(1)$ or even higher, which is beyond the scope of the current analysis.

4. Models of gas-cushioned droplet impact

For a gas-cushioned droplet impact of the form shown in figure 1(a), the droplet is assumed to be undeformed and circular when the separation between droplet and substrate is so large that there has been no opportunity for a build up of pressure in the gas film. Given the disparate horizontal and vertical scalings, a droplet (which is circular in dimensional variables), results in an undisturbed surface profile close to the bottom of the droplet with the form

$$f_+^{(0)}(x,\,t) = f^{(0)}(x,\,t) = \frac{x^2}{2} - t, \tag{4.1}$$

for large negative t. As time progresses the droplet free-surface is coupled to the pressure in the squeeze film through the integral equation (3.9), which takes the form

$$\frac{\partial^2 f^{(0)}}{\partial t^2} = \frac{1}{\pi} \fint_{-\infty}^{\infty} \frac{p_\xi^{(0)}\, d\xi}{\xi - x}. \tag{4.2}$$

for droplet impacts and is subject to the far-field conditions

$$f^{(0)}(x,\,t) \sim \frac{x^2}{2} - t \quad \text{and} \quad p^{(0)} \to 0, \quad \text{as} \quad |x| \to \infty. \tag{4.3}$$

The substrate that the droplet hits is flat and remains rigid throughout the impact, so that

$$f_-^{(0)}(x,\,t) = 0, \tag{4.4}$$

for all x and t. Although not included here, substrate roughness can be incorporated into the substrate via the method outlined by Hicks & Purvis (2010).

4.1. *Compressible gas regime*

If $Pe_g = O(1)$ and $K \sim \varepsilon$, so that there exists $\kappa = \varepsilon^{-1}K = O(1)$, then to leading-order in the gas energy conservation equation (2.11) implies

$$\frac{\partial^2 T_g^{(0)}}{\partial y^2} = 0. \tag{4.5}$$

This homogeneous partial differential equation must be solved subject to the Neumann boundary conditions (3.15*a*), giving a solution for the leading-order temperature profile

with the form $T_g^{(0)} = T_g^{(0)}(x, t)$. Therefore the leading-order temperature profile does not vary with height across the gas film. From the vertical momentum conservation equation in the gas film (3.4*b*), the gas pressure is also independent of the height across the gas film. In the equation of state, to leading order

$$1 + \kappa p^{(0)} = \rho_g^{(0)} \left(1 + \kappa T_g^{(0)}\right), \tag{4.6}$$

and consequently $\rho_g^{(0)} = \rho_g^{(0)}(x, t)$, so that the gas density is also independent of the height across the gas film. To leading order the gas viscosity equation is

$$1 + m\mu_g^{(0)} = \frac{\Theta\left(1 + \kappa T_g^{(0)}\right)^{3/2}}{\left(1 + \Pi + \kappa T_g^{(0)}\right)}, \tag{4.7}$$

and therefore $\mu_g^{(0)} = \mu_g^{(0)}(x, t)$ is also independent of the distance across the gas film.

Although the leading-order temperature has been shown to be independent of the gas-film height, the leading order behaviour of the energy conservation equation is insufficient to explicitly determine how $T_g^{(0)}$ varies with position along the gas film and time. Therefore it is necessary to proceed to higher order in ε in order to close the system of equations. At $O\left(\varepsilon^{-1}\right)$ a second homogeneous Neumann problem is again recovered with boundary conditions (3.15*b*), which has the solution $T_g^{(1)} = T_g^{(1)}(x, t)$. Again the first correction to the temperature profile is independent of height across the gas film. However, no further information about how $T_g^{(0)}$ varies along the gas film is gained at this level of approximation and it is necessary to continue to higher orders in ε to explicitly determine this dependence. Exploiting the fact the leading-order pressure and gas density are independent of the distance across the film height, at $O\left(\varepsilon^{0}\right)$, the energy conservation equation in the gas implies

$$\begin{aligned}\frac{1}{Pe_g}\frac{\partial^2 T_g^{(2)}}{\partial y^2} =& \rho_g^{(0)}\left(\frac{\partial T_g^{(0)}}{\partial t} + u_g^{(0)}\frac{\partial T_g^{(0)}}{\partial x}\right) - \frac{\gamma - 1}{\gamma}\left(\frac{\partial p^{(0)}}{\partial t} + u_g^{(0)}\frac{\partial p^{(0)}}{\partial x}\right) - \frac{1}{Pe_g}\frac{\partial^2 T_g^{(0)}}{\partial x^2} \\ &- \frac{\gamma - 1}{\gamma}\left(1 + m\mu_g^{(0)}\right)\left(\frac{\partial u_g^{(0)}}{\partial y}\right)^2,\end{aligned} \tag{4.8}$$

an inhomogenous Neumann problem, which must be solved subject to the boundary conditions (3.15*c*). A solution to this problem can only be obtained subject to a solvability condition, which is determined by integrating over the gas film height from the rigid substrate at $y = 0$ to the droplet free-surface at $y = f^{(0)}$. After this integration, the boundary conditions (3.15*c*) allow $T_g^{(2)}$ to be eliminated, leaving

$$\begin{aligned}&\rho_g^{(0)}\left(\frac{\partial T_g^{(0)}}{\partial t} + \frac{\partial T_g^{(0)}}{\partial x}\overline{u_g^{(0)}}\right) - \frac{\gamma - 1}{\gamma}\left(\frac{\partial p^{(0)}}{\partial t} + \frac{\partial p^{(0)}}{\partial x}\overline{u_g^{(0)}}\right) \\ &= \frac{1}{Pe_g f^{(0)}}\frac{\partial}{\partial x}\left[f^{(0)}\frac{\partial T_g^{(0)}}{\partial x}\right] + \frac{\gamma - 1}{\gamma}\left(1 + m\mu_g^{(0)}\right)\overline{\left(\frac{\partial u_g^{(0)}}{\partial y}\right)^2},\end{aligned} \tag{4.9}$$

where the average of a quantity over the film height is denoted

$$\overline{\chi} = \frac{1}{f^{(0)}}\int_0^{f^{(0)}} \chi \, \mathrm{d}y. \tag{4.10}$$

Consequently, calculating the average velocity over the gas film height provides

$$\overline{u_g^{(0)}} = -\frac{{f^{(0)}}^2}{12\left(1+m\mu_g^{(0)}\right)}\frac{\partial p^{(0)}}{\partial x}, \quad \text{and} \quad \overline{\left(\frac{\partial u_g^{(0)}}{\partial y}\right)^2} = \frac{{f^{(0)}}^2}{12\left(1+m\mu_g^{(0)}\right)^2}\left(\frac{\partial p^{(0)}}{\partial x}\right)^2. \quad (4.11)$$

Finally substituting into the energy conservation equation gives

$$\frac{\partial T_g^{(0)}}{\partial t} - \frac{{f^{(0)}}^2}{12\left(1+m\mu_g^{(0)}\right)}\frac{\partial p^{(0)}}{\partial x}\frac{\partial T_g^{(0)}}{\partial x} = \frac{1}{Pe_g\rho_g^{(0)}f^{(0)}}\frac{\partial}{\partial x}\left[f^{(0)}\frac{\partial T_g^{(0)}}{\partial x}\right] + \frac{\gamma-1}{\gamma\rho_g^{(0)}}\frac{\partial p^{(0)}}{\partial t}, \quad (4.12)$$

a non-linear advection-diffusion equation with source terms governing how the leading order gas temperature evolves. Using the gas mass and momentum conservation equations (3.2) and (3.4), the corresponding lubrication equation is given by

$$\frac{\partial}{\partial t}\left[\rho_g^{(0)}f^{(0)}\right] = \frac{1}{12}\frac{\partial}{\partial x}\left[\frac{\rho_g^{(0)}{f^{(0)}}^3}{\left(1+m\mu_g^{(0)}\right)}\frac{\partial p^{(0)}}{\partial x}\right], \quad (4.13)$$

where the leading-order gas density is given by (4.6) and the leading-order gas viscosity is related to the temperature through (4.7). The free-surface integral equation takes the form (4.2) for droplet impacts and together with equations (4.6) and (4.12-4.13) forms a closed system of four equations for the leading-order gas density, gas temperature, pressure and the free-surface profile.

Figure 2 illustrates the evolution in profiles of (a) the leading-order free-surface position, (b) the leading-order pressure, (c) the leading order gas temperature and (d) the leading order density at integer time increments over the course of a typical compressible gas cushioned droplet impact. The particular case shown has $\kappa = 0.5$ and $Pe_g = 7.5$, which corresponds to the impact of a droplet of radius $L = 0.1\,\text{mm}$ with an approach speed $U = 1.54\,\text{m}\,\text{s}^{-1}$. The free-surface and pressure profiles are qualitatively similar to results presented for the incompressible impact case (see e.g. Smith *et al.* 2003), with an initial increase in pressure below the minimum point of the droplet interface, which growing over time. This slows the descent of the droplet free-surface directly above this point, while away from its lowest point the free surface of the droplet continues to descend. The continued descent of the droplet free-surface away from the initial free-surface minimum coupled with the reduced speed of the free surface close to the initial minimum causes the free-surface to deform, which ultimately leads to touchdown some horizontal distance away from the point below the centre of the droplet and between these touchdown points a gas bubble is formed. Time is scaled so that in a vacuum the droplet would touchdown at $t = 0$. However, with air cushioning the droplet free-surface at $t = 0$ (indicated by the thin solid line in figure 2(a)), is still some distance above the solid body and, as with the incompressible case, the time at which touchdown occurs is delayed to a scaled time $t = 8$ (indicated by the thick solid line), after the time at which touchdown would have occurred in a vacuum. As initial touchdown approaches (at a time $t = 8$, and a horizontal distance $x = 5.35$ away from the undisturbed free-surface minimum), the droplet free-surface appears to tends to a cusp. In a small local region close to this point surface tension may re-emerge at leading order and thus play a role in the final rupture of the gas film. To the right of the free-surface minimum, the gas pressure rapidly decays and the free-surface profiles tend to the undisturbed far-field behaviour (4.3).

Unlike the incompressible case, the temperature and density profiles corresponding

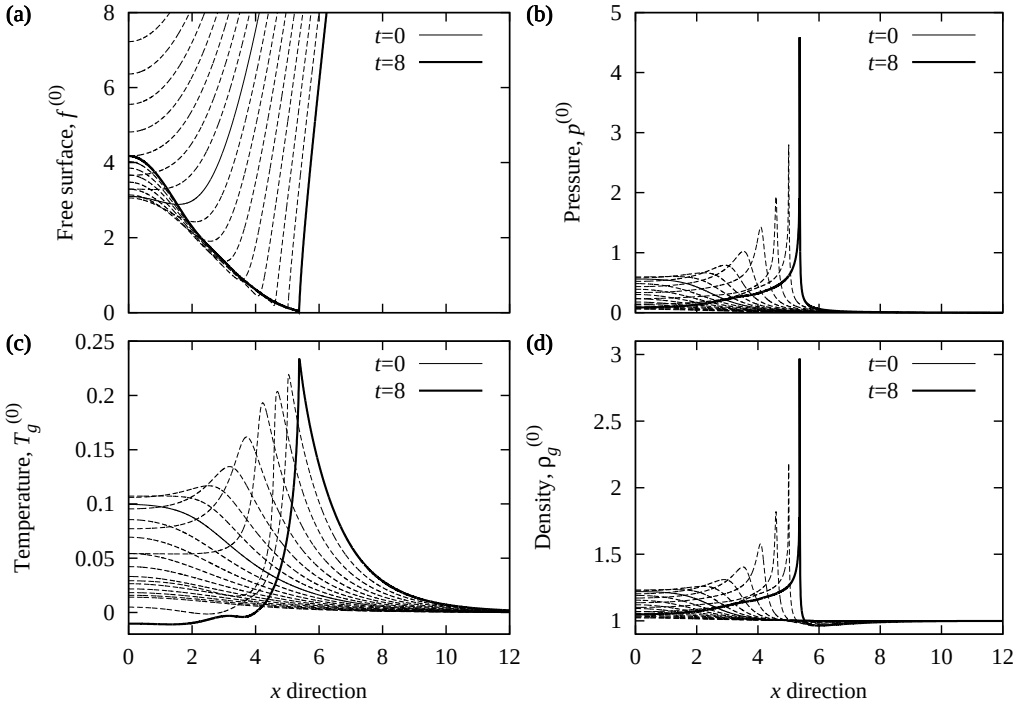

FIGURE 2. Profiles of (a) the leading-order free-surface position, (b) the leading-order pressure, (c) the leading order gas temperature and (d) the leading order density for a compressible gas-cushioned droplet impact with $\kappa = 0.5$ and $Pe_g = 7.5$ (corresponding to a droplet radius $L = 0.1\,\mathrm{mm}$ and impact speed $U = 1.54\,\mathrm{m\,s^{-1}}$). Results are shown at integer time increments with the thin solid line indicating the profiles at $t = 0$ (the time the droplet would touchdown in the absence of air cushioning), and the thick solid line showing the profile at the actual delayed instant of touchdown.

to a full analysis of the energy conservation equation can be seen for the first time. Following the pressure, both the temperature and gas density profiles initially increase directly below the oncoming droplet. However, the evolution of the free surface leads to a pair of maxima in both the gas temperature and density, which occur where the separation between the droplet and substrate is at a minimum. The gradients surrounding the pressure, gas density and gas temperature maxima differ due to the difference in the effective diffusion coefficients in (4.13) and (4.12), with increases in gas temperature occurring over a wider horizontal range due to heat diffusion. This diffusion of heat outside the confines of the trapped gas bubble leads to a small region with below ambient density just outside the touchdown point, created by the different rates at which the pressure and gas temperature approach their far-field values.

The same properties are shown in figure 3 for a range of different value of κ, while Pe_g remains fixed. The initial non-dimensional radius of the air pocket is independent of changes κ. This means that gas compressibility does not effect the initial radius of the air pocket, although the dimensional air pocket radius still increases with droplet radius L and decreases with impact speed U following the incompressible impact theory outlined by Hicks & Purvis (2010). Consequently the prediction of the incompressible theory, that

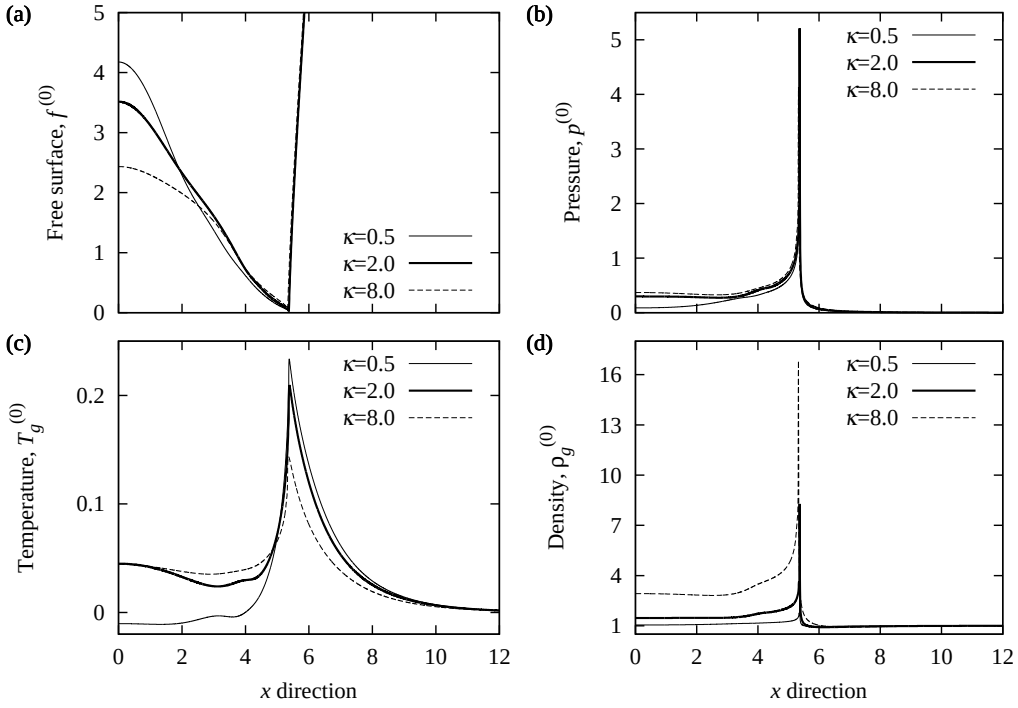

FIGURE 3. Profiles close to touchdown of (a) the leading-order free-surface position, (b) the leading-order pressure, (c) the leading order gas temperature and (d) the leading order density for a compressible gas-cushioned droplet impact. Profiles are shown for $Pe_g = 7.5$ with $\kappa = 0.5$ ($L = 0.103\,\mathrm{mm}$, $U = 1.54\,\mathrm{m\,s^{-1}}$), $\kappa = 2.0$ ($L = 0.052\,\mathrm{mm}$, $U = 3.09\,\mathrm{m\,s^{-1}}$) and $\kappa = 8.0$ ($L = 0.026\,\mathrm{mm}$, $U = 6.18\,\mathrm{m\,s^{-1}}$).

the radius of air pocket

$$r_p = r_p^\star \left(\frac{\mu_g L^2}{\rho_l U} \right)^{1/3}, \tag{4.14}$$

for a prefactor $r_p^\star$, persists upon entry to the compressible regime, with the value of the prefactor remaining unchanged. As the gas is known to compress as κ increases while the initial radius of the air pocket remains independent of κ, the initial height of the air pocket must decrease as κ rises. This is confirmed from the numerically computed free-surface profiles in figure 3(a), with the greatest reduction in height occurring directly below the centre of the droplet.

Figure 4 shows the solution profiles close to touchdown except that κ is fixed and the changes in the profile with variations in Pe_g are now illustrated. In this case the non-dimensional leading-order free-surface profile and pressure do not vary with changes in Pe_g, corresponding to the fact that Pe_g appears only in the energy conservation equation and not in the lubrication equation. Changing Pe_g does alter the non-dimensional leading-order temperature, with increases in Pe_g corresponding to a reduction in the thermal diffusion coefficient along the gap and a consequently a reduced lateral spreading of the heat generated by cushioning and a greater maximum temperature. Changes in Pe_g correspond to only small changes in the non-dimensional leading-order gas den-

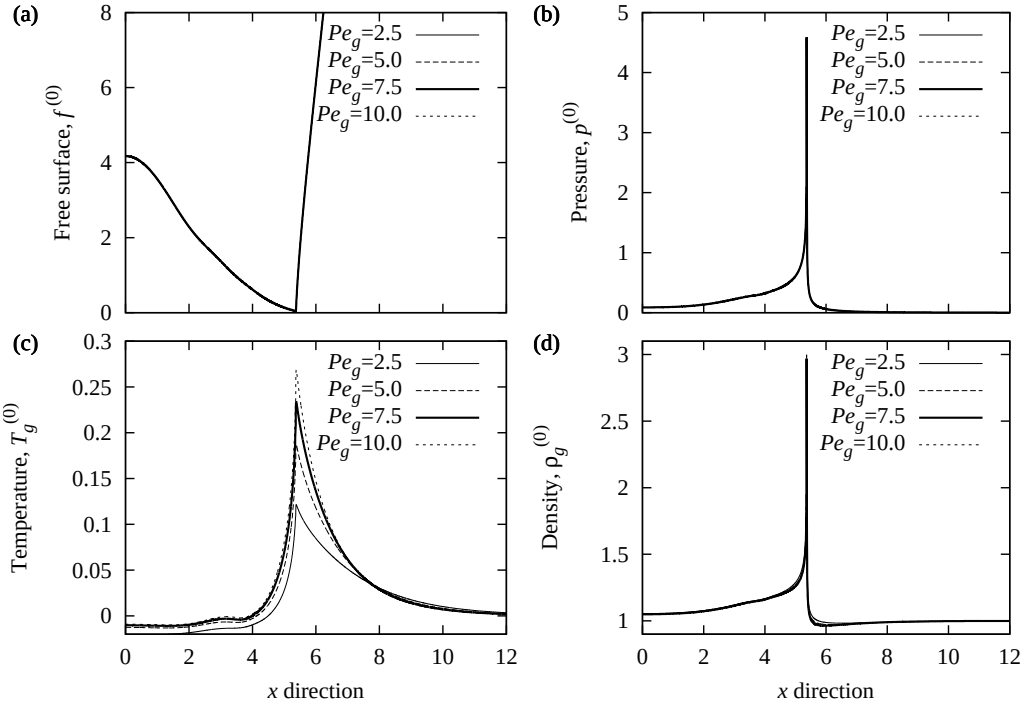

FIGURE 4. As figure 3, but showing $\kappa = 0.5$ and $Pe_g = 2.5$ ($L = 0.029\,\mathrm{mm}$, $U = 1.86\,\mathrm{m\,s^{-1}}$), $Pe_g = 5.0$ ($L = 0.064\,\mathrm{mm}$, $U = 1.65\,\mathrm{m\,s^{-1}}$), $Pe_g = 7.5$ ($L = 0.103\,\mathrm{mm}$, $U = 1.54\,\mathrm{m\,s^{-1}}$), and $Pe_g = 10.0$ ($L = 0.145\,\mathrm{mm}$, $U = 1.47\,\mathrm{m\,s^{-1}}$).

sity profile, with small changes being observed between the point of touchdown and the far-field conditions.

4.2. *Weakly compressible gas regime*

If $K \ll \varepsilon$, then from (2.16) the leading order equation of state for the gas is given by

$$\rho_g^{(0)} = 1. \tag{4.15}$$

In a similar way $\mu_g^{(0)} = 0$ to leading order. In this case the mass conservation equation for the gas (3.2) simplifies to give

$$\frac{\partial u_g^{(0)}}{\partial x} + \frac{\partial v_g^{(0)}}{\partial y} = 0, \tag{4.16}$$

while the leading order momentum conservation equations (3.4) also simplifies, leaving

$$0 = -\frac{\partial p^{(0)}}{\partial x} + \frac{\partial^2 u_g^{(0)}}{\partial y^2}, \tag{4.17a}$$

$$0 = -\frac{\partial p^{(0)}}{\partial y}. \tag{4.17b}$$

Hence the corresponding leading-order lubrication equation for droplet impact is

$$\frac{\partial f^{(0)}}{\partial t} = \frac{1}{12}\frac{\partial}{\partial x}\left[{f^{(0)}}^3 \frac{\partial p^{(0)}}{\partial x}\right], \tag{4.18}$$

while the free-surface profile is again coupled to the pressure through the integral condition (4.2). The combination of (4.18) and (4.2), exactly form the incompressible cushioning model first derived by Smith *et al.* (2003). Although this model is described as in the literature as the *incompressible* model, what is really meant is that variations in the gas density are at least an $O(\varepsilon)$ smaller than the gas pressure variations.

In particular, the correction to the constant density approximation at $O(\varepsilon)$ will be investigated in the case where $K = O(\varepsilon^2)$. Note from table 1 that a droplet with initial radius $L = 0.5\,\mathrm{mm}$ and approach speed $U = 0.3\,\mathrm{m\,s^{-1}}$, the compressibility parameter $\kappa = 0.018$ indicating compressibility is not very important and hence the leading-order pressure and free-surface evolution is governed by the closed system (4.18) and (4.2). If $K = \varepsilon^2 k$ where $k = O(1)$, then the equation of state (2.16) implies

$$1 + \varepsilon k p = \rho_g \left(1 + \varepsilon k T_g\right). \tag{4.19}$$

Upon substituting for the asymptotic expansions (3.1) and (3.10), the leading-order density is found to be given by (4.15). Proceeding to $O(\varepsilon)$, shows that the first correction to the constant density approximation is given by

$$\rho_g^{(1)} = k\left(p^{(0)} - T_g^{(0)}\right). \tag{4.20}$$

In the energy conservation equation (2.11), if the coefficients of ε are matched at $O(\varepsilon^{-2})$, then

$$\frac{\partial^2 T_g^{(0)}}{\partial y^2} = 0. \tag{4.21}$$

When subject to boundary condition (3.15*a*) this again forms a homegenous Neumann problem, with solutions of the form $T_g^{(0)} = T_g^{(0)}(x,\, t)$, i.e. the leading-order gas temperature is again independent of the height across the gap width. Proceeding to $O(\varepsilon^{-1})$

$$\frac{\partial^2 T_g^{(1)}}{\partial y^2} = 0, \tag{4.22}$$

subject to boundary conditions (3.15*b*). This again gives a homogeneous Neumann problem for $T_g^{(1)}$, with the for $T_g^{(1)} = T_g^{(1)}(x,\, t)$. Given the equation of state (4.20) and the vertical momentum conservation in the gas film (4.17*b*), the gas density $\rho_g^{(1)} = \rho_g^{(1)}(x,\, t)$. Matching coefficients at $O(1)$ gives

$$\begin{aligned}\frac{1}{Pe_g}\frac{\partial^2 T_g^{(2)}}{\partial y^2} = &\left(\frac{\partial T_g^{(0)}}{\partial t} + u_g^{(0)}\frac{\partial T_g^{(0)}}{\partial x}\right) - \frac{\gamma - 1}{\gamma}\left(\frac{\partial p^{(0)}}{\partial t} + u_g^{(0)}\frac{\partial p^{(0)}}{\partial x}\right) - \frac{1}{Pe_g}\frac{\partial^2 T_g^{(0)}}{\partial x^2} \\ &- \frac{\gamma - 1}{\gamma}\left(\frac{\partial u_g^{(0)}}{\partial y}\right)^2,\end{aligned} \tag{4.23}$$

an inhomogenous Neumann problem, which is again subject to the boundary conditions (3.15*c*). A solution to this problem only exists if a solvability condition is satisfied. Again this condition is obtained by integrating from $y = 0$ to $y = f^{(0)}$. Subsequently substituting for the average velocity fluxes from the appropriately modified versions of (4.11) gives

$$\frac{\partial T_g^{(0)}}{\partial t} - \frac{{f^{(0)}}^2}{12}\frac{\partial p^{(0)}}{\partial x}\frac{\partial T_g^{(0)}}{\partial x} = \frac{1}{Pe_g f^{(0)}}\frac{\partial}{\partial x}\left[f^{(0)}\frac{\partial T_g^{(0)}}{\partial x}\right] + \frac{\gamma - 1}{\gamma}\frac{\partial p^{(0)}}{\partial t}, \tag{4.24}$$

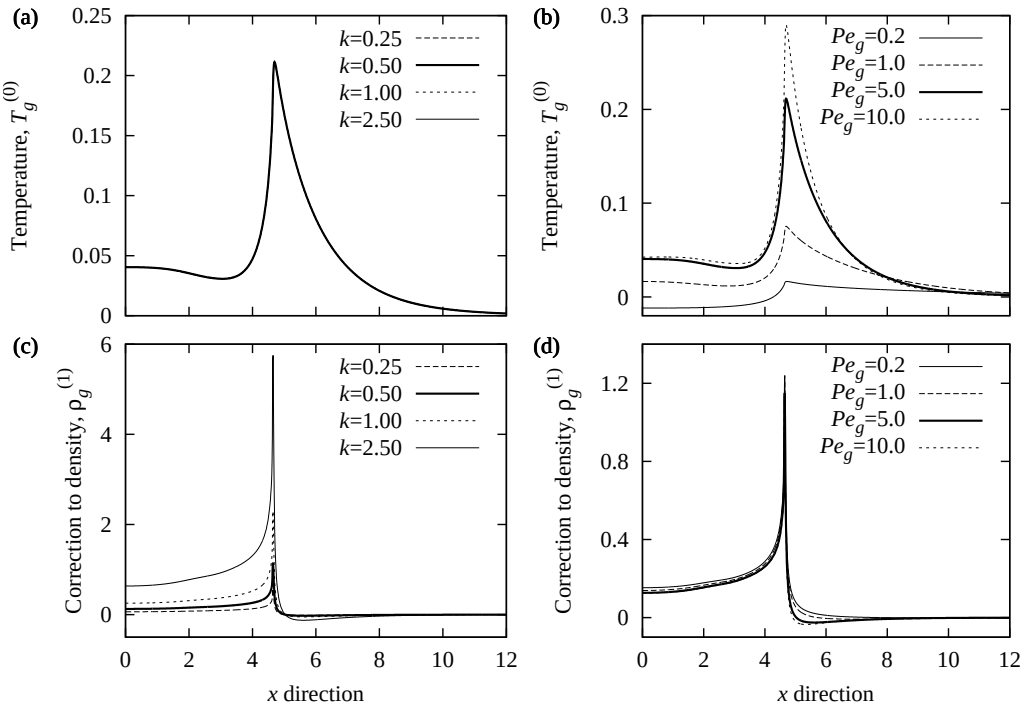

FIGURE 5. The leading-order temperature profile (top) and the first correction to the gas density (bottom) at touchdown in weakly compressible gas-cushioned droplet impacts for variations in k with $Pe_g = 5$ fixed (left) and for variations in Pe_g with $k = 0.5$ fixed (right).

an advection-diffusion equation with source terms for the leading-order gas temperature $T_g^{(0)}$. Having determined the leading-order free-surface and pressure profiles from (4.18) and (4.2), this solvability condition can be used to calculate the correction to the leading-order gas temperature and subsequently the first correction to the gas density can be determined from (4.20).

The evolution in the free-surface profile and gas properties as a droplet approaches touchdown when cushioned by a weakly compressible gas a qualitatively similar to the results presented for the fully compressible case, except for the gas density correction, which now evolves from zero and tends to zero in the far-field, unlike the leading-order gas density of the fully compressible case which uniformly takes the value one before being disturbed. The free surface again evolves to trap a small gas pocket, which subsequently can evolve into a trapped gas bubble.

Figure 5 illustrates how variations in k and Pe_g effect the leading-order gas temperature and the first correction to the constant gas density. Figures 5(a) and (c) illustrate the changes in the gas temperature and the gas density correction at touchdown for a range of values of $k = \varepsilon^{-2}K$ while Pe_g remains fixed, while conversely figures 5(b) and (d) show the change in touchdown profile for fixed k as Pe_g varies. For fixed Pe_g the gas temperature profile appears independent of k in the range tested, while larger values of k correspond to the largest increases in density, which is consistent with a return to the compressible regime for large k. For fixed k, increases in Pe_g act to reduce the effective thermal diffusion coefficient along the gas film, which results in much higher temperature maxima. For low values of Pe_g the thermal diffusion along the gas film is significant and

the increases in gas temperature close to the point of touchdown are reduced as the heat diffuses along the gas film.

5. Models of gas-cushioned solid body impact into water

The bottom of a circular body with radius of curvature L and approach speed U, has the scaled non-dimensional profile

$$f_+^{(0)}(x,\,t) = s(x,\,t) = \frac{x^2}{2} - t, \tag{5.1}$$

for all x and t as it approaches impact with the liquid. For large negative t, the gas squeeze film does not experience a build up of pressure and so initially the liquid free-surface

$$f_-^{(0)}(x,\,t) = h(x,\,t) = 0. \tag{5.2}$$

However, as impact is approached the motion of the free surface is governed by the integral equation (3.9), which takes the form

$$\frac{\partial^2 f_-^{(0)}}{\partial t^2} = \frac{\partial^2 h^{(0)}}{\partial t^2} = -\frac{1}{\pi}\int_{-\infty}^{\infty} \frac{p_\xi^{(0)}\,d\xi}{\xi - x}, \tag{5.3}$$

in response to the increase in gas pressure, while in the far-field

$$f_-^{(0)}(x,\,t) = h(x,\,t) \to 0 \quad \text{and} \quad p^{(0)} \to 0, \quad \text{as} \quad |x| \to \infty. \tag{5.4}$$

An analysis for weakly-compressible impacts with $k = O(1)$ and $\widetilde{Pe}_g = \varepsilon Pe_g = O(1)$ has previously been conducted by Hicks & Purvis (2012). Consequently in this section the focus is on fully compressible impacts in which $\kappa = O(1)$ and $\widetilde{Pe}_g = O(1)$. In this case the leading-order behaviour of the gas energy conservation equation (2.11) again implies $T_g^{(0)} = T_g^{(0)}(x,\,t)$ as a result of the boundary conditions (3.15a). Therefore the leading-order temperature profile does not vary with height across the gas film and it is again necessary to proceed to higher orders in ε to close the problem. In this limit, the vertical momentum conservation equation in the gas film (3.4b) again implies that the gas pressure is also independent of the height across the gas film and consequently the leading-order gas density and viscosity satisfy (4.6) and (4.7), respectively.

Continuing with the expansion to next order,

$$\begin{aligned}\frac{1}{\widetilde{Pe}_g}\frac{\partial^2 T_g^{(1)}}{\partial y^2} =& \rho_g^{(0)}\left(\frac{\partial T_g^{(0)}}{\partial t} + u_g^{(0)}\frac{\partial T_g^{(0)}}{\partial x}\right) - \frac{\gamma-1}{\gamma}\left(\frac{\partial p^{(0)}}{\partial t} + u_g^{(0)}\frac{\partial p^{(0)}}{\partial x}\right)\\ &- \frac{\gamma-1}{\gamma}\left(1 + m\mu_g^{(0)}\right)\left(\frac{\partial u_g^{(0)}}{\partial y}\right)^2,\end{aligned} \tag{5.5}$$

an inhomogenous Neumann problem when subject to the boundary conditions (3.15b). In this expression $T_g^{(1)}$ can be eliminated by integrating over the gas film height from the liquid free-surface $y = h^{(0)}$ to the solid body $y = s^{(0)}$. Performing this integration

$$\begin{aligned}\rho_g^{(0)}\left(\frac{\partial T_g^{(0)}}{\partial t} + \overline{u_g^{(0)}}\frac{\partial T_g^{(0)}}{\partial x}\right) - \frac{\gamma-1}{\gamma}\left(\frac{\partial p^{(0)}}{\partial t} + \overline{u_g^{(0)}}\frac{\partial p^{(0)}}{\partial x}\right)&\\ = \frac{\gamma-1}{\gamma}\left(1 + m\mu_g^{(0)}\right)\overline{\left(\frac{\partial u_g^{(0)}}{\partial y}\right)^2},&\end{aligned} \tag{5.6}$$

where the average of a quantity across the gas film is given by

$$\overline{\chi} = \frac{1}{s - h^{(0)}} \int_{h^{(0)}}^{s} \chi \, \mathrm{d}y, \tag{5.7}$$

Consequently, calculating the average velocity over the gas film height provides

$$\overline{u_g^{(0)}} = -\frac{\left(s - h^{(0)}\right)^2}{12\left(1 + m\mu_g^{(0)}\right)} \frac{\partial p^{(0)}}{\partial x}, \quad \text{and} \quad \overline{\left(\frac{\partial u_g^{(0)}}{\partial y}\right)^2} = \frac{\left(s - h^{(0)}\right)^2}{12\left(1 + m\mu_g^{(0)}\right)^2} \left(\frac{\partial p^{(0)}}{\partial x}\right)^2. \tag{5.8}$$

Substituting for the averaged velocities from (5.8) gives

$$\frac{\partial T_g^{(0)}}{\partial t} - \frac{\left(s - h^{(0)}\right)^2}{12\left(1 + m\mu_g^{(0)}\right)} \frac{\partial p^{(0)}}{\partial x} \frac{\partial T_g^{(0)}}{\partial x} = \frac{\gamma - 1}{\gamma \rho_g^{(0)}} \frac{\partial p^{(0)}}{\partial t}, \tag{5.9}$$

another advection-diffusion equation with source terms, governing the evolution of the leading-order gas temperature. Note that for the larger body impacts of interest here (unlike the earlier smaller droplet impact problem), curvature effects do not enter the heat flux boundary conditions before $T_g^{(0)}$ can be determined.

In this case the mass and momentum equations imply

$$\frac{\partial}{\partial t}\left[\rho_g^{(0)}\left(s - h^{(0)}\right)\right] = \frac{1}{12}\frac{\partial}{\partial x}\left[\frac{\rho_g^{(0)}\left(s - h^{(0)}\right)^3}{\left(1 + m\mu_g^{(0)}\right)} \frac{\partial p^{(0)}}{\partial x}\right], \tag{5.10}$$

Together with the free-surface integral equation (5.3), the equations (4.6), (4.7), (5.9) and (5.10) form a closed system of equations for the leading-order gas density, gas temperature, gas viscosity, pressure and the free-surface profile.

The evolution of (a) the solid body and leading-order free-surface position, (b) the leading-order pressure, (c) the leading-order gas temperature and (d) the leading-order gas density are shown in figure 6 for a solid body approaching impact with a liquid separated by a fully compressible gas phase. In this case, as the solid body approaches impact with the liquid, the pressure in the gas rises as it is both compressed and forced out of the way. This initially presses down on the liquid free-surface, causing it to deform out of the path of the oncoming solid. Subsequently liquid mass conservation causes the free-surface to rise above its undisturbed level some horizontal distance away from the initial downwards deflection of the free surface. Touchdown is again delayed. The leading-order pressure, gas temperature and gas density have maxima at the location of the closest separation between solid and liquid. The temperature maxima have wider lateral support than the pressure maxima due to the thermal diffusion in the energy conservation equations. This leads to a small region of below ambient gas density just outside the region of touchdown.

Figure 7 shows the variation in dimensional profiles close to the initial point of touchdown for a solid body with a radius of curvature $L = 0.05\,\mathrm{m}$ and a range of impact speeds U between 0.4 and $2\,\mathrm{m\,s^{-1}}$. As with the compressible droplet impact case the initial radius of the trapped air pocket again matches the predictions of the incompressible theory of Hicks *et al.* (2012). However, the results again show that the height of the gas pocket falls with increasing impact speed, both in term of the absolute height and the height compared to the incompressible predictions, indicating the gas is compressed. As one would expect higher pressures are obtained with higher impact speeds, while gas

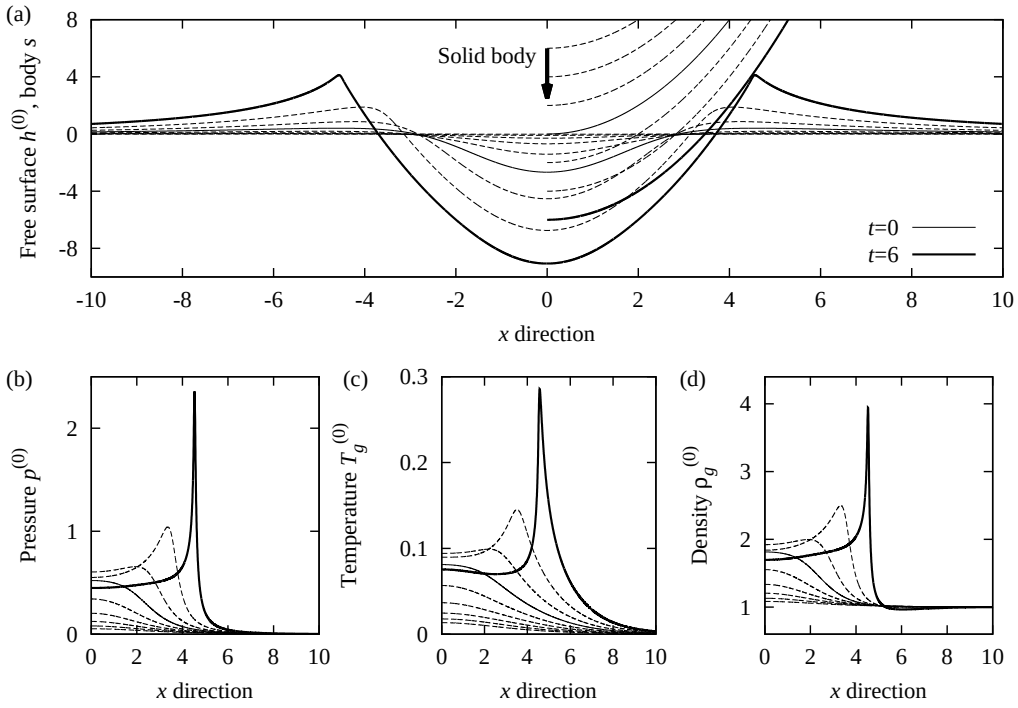

FIGURE 6. Profiles of (a) the solid body position and the leading-order free-surface position, (b) the leading-order pressure, (c) the leading-order gas temperature and (d) the leading-order gas density for a compressible gas-cushioned impact of a solid body into a liquid with $L = 0.05\,\mathrm{m}$ and $U = 1.2\,\mathrm{m\,s^{-1}}$ (corresponding to $\kappa = 2.18$ and $\widetilde{Pe}_g = 18.6$. Results are shown at two integer time increments with the thin solid line indicating the profiles at $t = 0$. For clarity only the body shapes for positive values of x are shown.

temperature and density also increases with impact speed due to an increase both in the work done compressing the gas and in viscous heating. Increases in U for fixed L correspond to increases in both κ and $\widetilde{Pe}_g$.

6. Conclusions and further discussion

New models for a range of compressible gas-cushioned liquid-solid impacts have been proposed, which can be applied to both droplet impacts and the impact of solid bodies into water. Unlike existing models of compressible gas cushioned liquid-solid impacts, a full analysis of the energy conservation has been incorporated for the first time and this has shown that the previous use of either an isothermal or an adiabatic equation of state is inappropriate in this regime.

To assess what difference a full analysis of the energy conservation makes compared to either an adiabatic or isothermal equation of state for the gas, the results of the current theory for droplet impacts are compared with the earlier models. In the current notation the free-surface profile $f^{(0)}$ and pressure $p^{(0)}$, associated with the earlier adiabatic and isothermal models of Mandre *et al.* (2009) and Mani *et al.* (2010) are related through

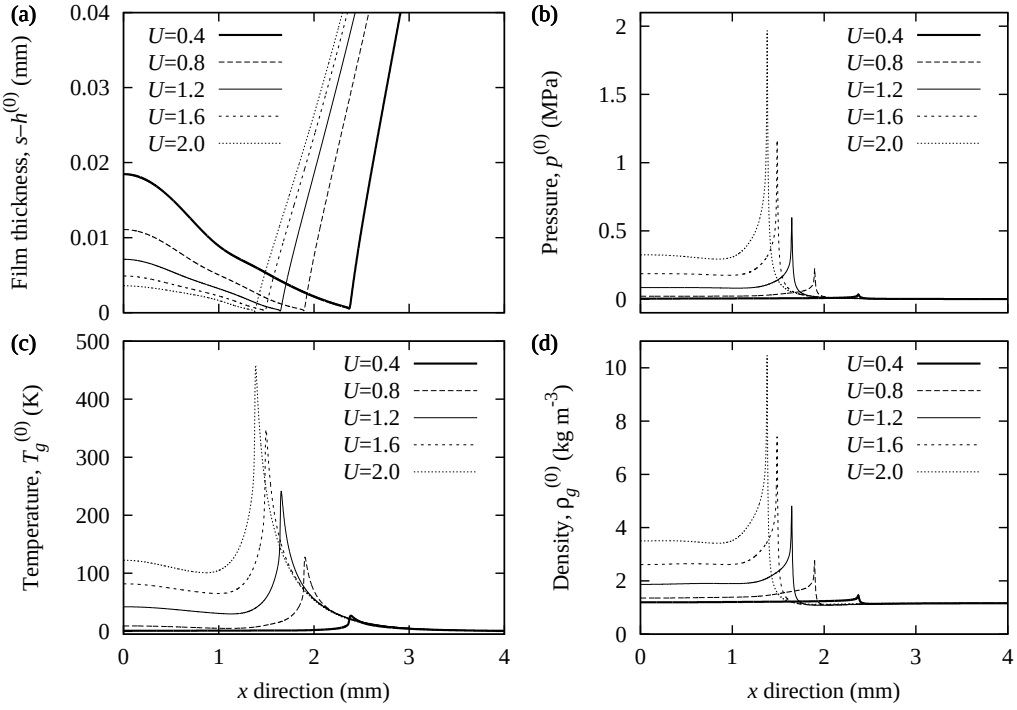

FIGURE 7. Profiles of (a) the leading-order separation between the solid body and the free-surface position, (b) the leading-order pressure, (c) the leading order gas temperature and (d) the leading order density for a compressible gas-cushioned solid body of radius $L = 0.05\,\mathrm{m}$, impacting into water with velocity $U = 0.4\,\mathrm{m\,s^{-1}}$ ($\kappa = 0.168$, $\widetilde{Pe}_g = 8.96$), $U = 0.8\,\mathrm{m\,s^{-1}}$ ($\kappa = 0.845$, $\widetilde{Pe}_g = 14.2$), $U = 1.2\,\mathrm{m\,s^{-1}}$ ($\kappa = 2.18$, $\widetilde{Pe}_g = 18.6$), $U = 1.6\,\mathrm{m\,s^{-1}}$ ($\kappa = 4.26$, $\widetilde{Pe}_g = 22.6$) and $U = 2.0\,\mathrm{m\,s^{-1}}$ ($\kappa = 7.17$, $\widetilde{Pe}_g = 26.2$).

equations (4.13) and (4.2), while the gas density is given by

$$\rho_g^{(0)} = \left(1 + \kappa p^{(0)}\right)^{\gamma}, \tag{6.1}$$

with $\gamma = 1.4$ in the adiabatic case and $\gamma = 1$ in the isothermal case. Equation (4.13) additionally includes temperature dependent viscosity, which was not incorporated into the earlier models.

Figure 8 shows profiles at touchdown corresponding to a full analysis of the energy conservation equation, an adiabatic equation of state and an isothermal equation of state. In the case of the full model and the isothermal model results are presented for $\kappa = 2$, while in the adiabatic case the results are additionally presented for $\kappa = 0.5$. The results of the full analysis are presented for $Pe_g = 7.5$. Coincidentally the maximum temperature predicted in this case is close to that given by the adiabatic model. However, for cushioning with an adiabatic or isothermal equation of state, the choice $\kappa = 2$ determines a particular impact speed U for *each* choice of L across the range of applicability of the theory. With the full analysis of the energy conservation, the additional choice of Pe_g, uniquely determines both the impact speed and radius of curvature: in this case $U = 3.09\,\mathrm{m\,s^{-1}}$ while $L = 0.052\,\mathrm{mm}$.

The key differences between the current compressible models and the earlier isentropic

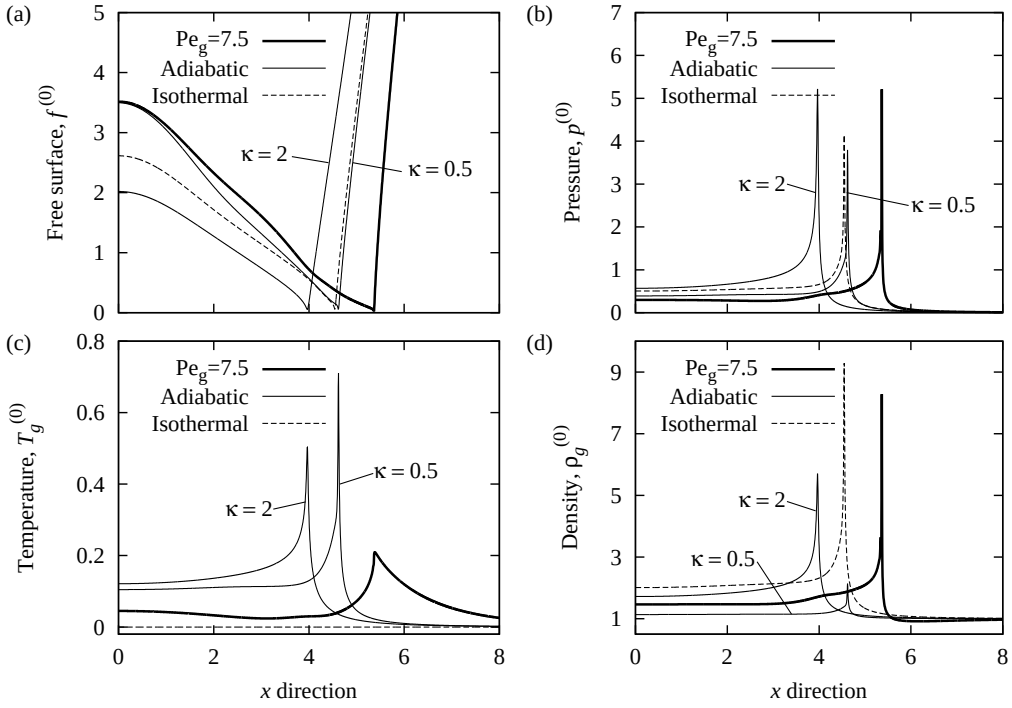

FIGURE 8. As figure 3, but showing profiles calculated using the full energy conservation equation with $\kappa = 2$ and $Pe_g = 7.5$, an adiabatic equation of state with $\kappa = 2$ and with $\kappa = 0.5$ and an isothermal equation of state with $\kappa = 2$.

and isothermal theories are apparent in the temperature profiles. The current model, which incorporates the full energy conservation equation produces temperature profiles that change over time unlike profiles generated in the isothermal case. The temperature maxima generated by the full theory are broader and more diffuse than those created through the use of an adiabatic equation of state. Figure 4 indicates that increases in Pe_g (which correspond to a decreases in the effective temperature diffusion coefficient), will produce higher maximum temperatures as the heat energy generated is less able to diffuse away from the point of touchdown. Conversely decreases in Pe_g (which correspond to an increases in the effective temperature diffusion coefficient), produce lower maximum temperatures as the heat energy generated is more able to diffuse away from the point of touchdown. Therefore by increasing or decreases Pe_g, temperature profiles can be generated with temperature maxima either above or below those found for an isentropic impact with the equivalent value of κ. However, for given fluid properties, the impact parameters L and U uniquely determine both κ and Pe_g. Therefore while there may be impacts in which the use of either an adiabatic or an isothermal equation of state may roughly approximate the correct temperature profile, in general a deeper analysis of energy conservation is required.

The second key difference between the results from the full model and the earlier isentropic and isothermal theories is present in the density profiles, which in the case of a full analysis of the energy conservation equation can take below ambient values for horizontal locations just beyond the droplet free-surface minima. These below ambient densities are not formed in either the adiabatic or incompressible cases, as in these cases

the gas density is a monotonically increasing function of the gas pressure, which itself is non-negative in normal liquid-solid impacts. However, in the full model the enhanced lateral diffusion of heat energy about the temperature maximum, coupled to the pressure via the ideal gas equation can produce below ambient gas densities.

The final key difference between the current model and the earlier isentropic studies is that, in the adiabatic case, the initial air pocket radius decreases as κ rises, as indicated by the $\kappa = 0.5$ and 2 profiles in figure 8. This differs from the behaviour seen in the full analysis (as presented in figure 3), where the initial radius of the air pocket is independent of κ. The greater lateral spreading associated with a full analysis of the energy conservation equation compared to either the adiabatic or the isothermal cases, results in a larger initial gas pocket radius. This is a result of interactions of between the gas density, temperature and steeper slope on the free surface in this region. Together these factors contribute to an effective diffusion coefficient $\rho_g^{(0)} {f^{(0)}}^3/12$, in (4.13), which promotes the lateral spreading of the droplet. If the initial gas pocket radius is independent of κ once the theory is extended to axisymmetry, then experimentally measuring the initial radius of an air pocket in the compressible regime provides a means of validating the developed theory. This is because the functional dependence of the initial air pocket radius r_p upon U and R is given equation (4.14) in both two-dimensional and axisymmetric geometries. The difference between the two geometries is the value of the prefactor $r_p^\star$. Equation (4.14) has been successfully validated in the incompressible regime where excellent agreement is obtained with experiments (Hicks *et al.* 2012). However, if the gas really does behave either adiabatically or isothermally in the compressible regime, then experimentally measured initial trapped gas pocket radii should be less than the incompressible predictions, while if the full analysis presented holds, then the incompressible predictions are expected to hold.

The inclusion of temperature dependent gas viscosity results in a 4% increase in the volume of the gas pocket in the full model and a 6% increase in the volume of the gas pocket in the adiabatic model, for the results presented in figure 8 with $\kappa = 2$, compared to the equivalent model with constant viscosity. The profiles between those with and without temperature dependent viscosity increase with κ. However, these changes are so small in the range of interest that the results are not presented.

Recently developed experimental techniques such as optical interferometry have captured the free-surface profile as a droplet entrains a bubble during a gas cushioned impact (Dell'Aversana *et al.* 1997; Driscoll & Nagel 2011; van der Veen *et al.* 2012; Liu *et al.* 2013). Quantitative comparisons of the current compressible theory against droplet impact experiments are not yet possible because interferometry profiles have not been published alongside the radius of curvature at the bottom of the droplet just prior to cushioning. Due to the oscillations of a free falling droplet, this key length scale can vary significantly from the undisturbed droplet radius (Thoroddsen *et al.* 2005). Additionally the current theory is limited to two spatial dimensions and would need to be extended to cover axisymmetric geometries to enable direct quantitative comparisons. However, these comparisons remain a goal for future work as and when suitable experimental data becomes available. Direct measurements of the pressure evolution in a gas-cushioned impact give good qualitatively agreement with theoretical computations (Lesser & Field 1983). However, such measurements require highly sensitive pressure sensors and more recent experimental studies have not tried to directly measure the pressure in spite of the fact there are many applications, such as surface erosion by droplet impacts, where the pressure distribution is arguably of more importance than the free-surface profile. For the first time the current work links the free-surface profile and pressure with the

gas temperature and density in a manor consistent with a full analysis of the energy conservation equation. High speed optical cameras have captured the evolution of the free surface and it would be very interesting to see whether high speed infra-red cameras can capture the spatial and temporal temperature evolution. The improved understanding on the relationship between temperature and pressure in gas cushioned impacts potentially opens up new avenues for experimental determination of the pressure profile which could be calculated from the temperature profile.

The theory describes gas cushioning for liquid-solid impacts in which either $Pe_g = O(1)$ or $\widetilde{Pe}_g = O(1)$. For impacts of larger bodies with higher momentum $\varepsilon^2 Pe_g$ could be $O(1)$ or higher. As an example of an impact in this regime, a body with radius of curvature $L = 4\,\mathrm{m}$ and an approach speed $U = 5\,\mathrm{m\,s^{-1}}$, corresponding to an impact which may be expected in ship slamming gives $\varepsilon^2 Pe_g = 0.86$, indicating that thermal diffusion across the gap no longer dominates the energy conservation equation. In this regime the leading-order gas temperature satisfies an inhomogeneous Neumann problem allowing the gas temperature to vary across the height of the gap. For impacts of this size or even droplet impacts with much higher velocities $\kappa \gg 1$, indicating that gas compression dominates lateral motion in the squeeze film. A full analysis of the energy conservation equations in these physically significant regimes remains an interesting candidate for further study.

REFERENCES

Abrahamsen, Bjørn C. & Faltinsen, Odd M. 2011 The effect of air leakage and heat exchange on the decay of entrapped air pocket slamming oscillations. *Phys. Fluids* **23** (10), 102107.

Baldessari, F., Homsy, G. M. & Leal, L. G. 2007 Linear stability of a draining film squeezed between two approaching droplets. *J. Colloid Interface Sci.* **307** (1), 188–202.

Batchelor, G. K. 1967 *An Introduction to Fluid Dynamics*. Cambridge University Press, Cambridge, United Kingdom.

Bhardwaj, Rajneesh & Attinger, Daniel 2008 Non-isothermal wetting during impact of millimeter-size water drop on a flat substrate: Numerical investigation and comparison with high-speed visualization experiments. *Int. J. Heat Fluid Flow* **29** (5), 1422–1435.

Bhardwaj, R., Longtin, J. P. & Attinger, D. 2007 A numerical investigation on the influence of liquid properties and interfacial heat transfer during microdroplet deposition onto a glass substrate. *Int. J. Heat Mass Trans.* **50** (15–16), 2912–2923.

Brenner, Michael P., Hilgenfeldt, Sascha & Lohse, Detlef 2002 Single-bubble sonoluminescence. *Rev. Mod. Phys.* **74** (2), 425–484.

Chuang, S.-L. 1966 Experiments on flat-bottom slamming. *J. Ship Res.* **10**, 10–17.

Colagrossi, A., Lugni, C., Greco, M. & Faltinsen, O. M. 2004 Experimental and numerical investigation of 2d sloshing with slamming. In *In proceedings of 19th Workshop on Water Waves and Floating Bodies, Cortona, Italy* (ed. M. Landrini, E. F. Campana & A. Iafrati).

van Dam, D. B. & Le Clerc, C. 2004 Experimental study of the impact of an ink-jet printed droplet on a solid substrate. *Phys. Fluids* **16** (9), 3403–3414.

Dell'Aversana, P., Tontodonato, V. & Carotenuto, L. 1997 Suppression of coalescence and of wetting: The shape of the interstitial film. *Phys. Fluids* **9** (9), 2475–2485.

Driscoll, Michelle M. & Nagel, Sidney R. 2011 Ultrafast interference imaging of air in splashing dynamics. *Phys. Rev. Lett.* **107** (15), 154502.

Gent, R. W., Dart, N. P. & Cansdale, J. T. 2000 Aircraft icing. *Phil. Trans. R. Soc. Lond. A* **359**, 2873–2911.

Hicks, P. D., Ermanyuk, E. V., Gavrilov, N. V. & Purvis, R. 2012 Air trapping at impact of a rigid sphere onto a liquid. *J. Fluid Mech.* **695**, 310–320.

Hicks, P. D. & Purvis, R. 2010 Air cushioning and bubble entrapment in three-dimensional droplet impacts. *J. Fluid Mech.* **649**, 135–163.

Hicks, P. D. & Purvis, R. 2011 Air cushioning in droplet impacts with liquid layers and other droplets. *Phys. Fluids* **23** (6), 062104.

Hicks, Peter D. & Purvis, Richard 2012 Compressible air cushioning in liquid-solid impacts. In *Proceedings of 2nd International Conference on Violent Flows, Nantes, 25–27 September*.

Howell, P. D. 2001 *Mathematical Modeling: Case Studies from Industry*, chap. 1 - Fluid-Mechanical Modelling of the Scroll Compressor, pp. 22–45. Cambridge University Press, Cambridge, United Kingdom.

Kaur, S. & Leal, L. G. 2009 Three-dimensional stability of a thin film between two approaching drops. *Phys. Fluids* **21** (7), 072101.

Lesser, M. B. & Field, J. E. 1983 The impact of compressible liquids. *Annu. Rev. Fluid Mech.* **15**, 97–122.

Liu, Yuan, Tan, Peng & Xu, Lei 2013 Compressible air entrapment in high-speed drop impacts on solid surfaces. *J. Fluid Mech.* **716**, R9.

Mandre, S., Mani, M. & Brenner, M. P. 2009 Precursors to splashing of liquid droplets on a solid surface. *Phys. Rev. Lett.* **102** (13), 134502.

Mani, M., Mandre, S. & Brenner, M. P. 2010 Events before droplet splashing on a solid surface. *J. Fluid Mech.* **647**, 163–185.

Marston, J. O., Vakarelski, I. U. & Thoroddsen, S. T. 2011 Bubble entrapment during sphere impact onto quiescent liquid surfaces. *J. Fluid Mech.* **680**, 660–670.

Oliver, J. M. 2002 Water entry and related problems. PhD thesis, University of Oxford, Oxford, United Kingdom.

Purvis, R. & Smith, F. T. 2004 Air-water interactions near droplet impact. *Eur. J. Appl. Math.* **15**, 853–871.

Rognebakke, O. F. & Faltinsen, O. M. 2005 Sloshing induced impact with air cavity in rectangular tank with a high filling ratio. In *In proceedings of the 20th International Workshop on Water Waves and Floating Bodies* (ed. J. Grue).

Rohsenow, Warren M., Hartnett, James P. & Cho, Young I., ed. 1998 *Handbook of Heat Transfer*, Third edn. McGraw-Hill, Boston.

Smith, F. T., Li, L. & Wu, G. X. 2003 Air cushioning with a lubrication/inviscid balance. *J. Fluid Mech.* **482**, 291–318.

Stewartson, K. 1964 *The theory of laminar boundary layers in compressible fluids*. Oxford Clarendon Press, Oxford, United Kingdom.

Takagi, K. & Dobashi, J. 2003 Influence of trapped air on the slamming of a ship. *J. Ship Res.* **47** (3), 187–193.

Thoroddsen, S. T., Etoh, T. G. & Takehara, K. 2003 Air entrapment under an impacting drop. *J. Fluid Mech.* **478**, 125–134.

Thoroddsen, S. T., Etoh, T. G., Takehara, K., Ootsuka, N. & Hatsuki, Y. 2005 The air bubble entrapped under a drop impacting on a solid surface. *J. Fluid Mech.* **545**, 203–212.

van der Veen, R. C. A., Tran, T., Lohse, D. & Sun, C. 2012 Direct measurements of air layer profiles under impacting droplets using high-speed color interferometry. *Phys. Rev. E* **85**, 026315.

Wilson, S. K. 1991 A mathematical model for the initial stages of fluid impact in the presence of a cushioning fluid layer. *J. Eng. Math.* **25** (3), 265–285.

Xu, L., Zhang, W. W. & Nagel, S. R. 2005 Drop splashing on a dry smooth surface. *Phys. Rev. Lett.* **94**, 184505.